SATELLITE PRODUCTS AND SERVICES REVIEW BOARD

ATBD: Satellite-Derived Oceanic Heat Content

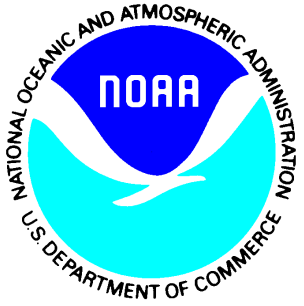

Version 3.3

October 2022

TITLE: ALGORITHM THEORETICAL BASIS DOCUMENT FOR SATELLITE DERIVED OCEANIC HEAT CONTENT PRODUCT VERSION 3.3

AUTHORS:

Lynn K. Shay and Jodi K. Brewster (RSMAS/ University of Miami)

Eileen Maturi and David Donahue (NOAA NESDIS/STAR)

Patrick Meyers and Claire McCaskill (RSMAS/University of Miami)

TABLE OF CONTENTS

LIST OF TABLES AND FIGURES

Page

LIST OF ACRONYMS

AMSR: Advanced Microwave Sounding Radiometer
AXBT : Airborne Expendable Bathythermograph
AXCP: Airborne Expendable Current Profiler
AXCTD: Airborne Expendable Conductivity Temperature Depth profiler
CCR: Cold Core Rings
D20: Depth of the 20ºC isotherm (H20)
D26: Depth of the 26ºC isotherm (H26)
Envisat: Environmental Satellite
EPAC: Eastern Pacific Ocean
EPIC : Eastern Pacific Investigation of Climate
FC: Florida Current
GCW: Gulf of Mexico Common water
GDEM: Generalized Digital Environmental Model
GOM: Gulf of Mexico
GPS: Global Positioning System
GS: Gulf Stream
HYCOM: Hybrid Coordinate Ocean Model
IFEX: Intensity Fluctuation Experiment
LC: Loop Current
OHC: Oceanic Heat Content
OA: Objective Analysis
OSTP: Ocean Surface Topography Program
PIRATA: Pilot Research Moored Array in tropical Atlantic
MLD : Mixed Layer Depth
MLT : Mixed Layer Temperature
MPI: Maximum Potential Intensity
NASA : National Aeronautics and Space Administration
NRL : US Navy Research Laboratories
PSU : Practical Salinity Unit (psu)
RMSD: Root mean squared difference
SSHA: Sea-Surface Height Anomaly
SSH: Sea-Surface Height
SHIPS: Statistical Hurricane Intensity Prediction Scheme
SAAIW: Subsurface Antarctic Intermediate Water
SST: Sea Surface Temperature
STW: Subtropical Water
TOPEX: The Topographic Experiment (Radar Altimeter)
TMI: Tropical Rain Measuring Mission (TRMM) Microwave Imager
WCR: warm core rings
WOA: World Ocean Atlas
XBT: Expendable Bathythermographs

ABSTRACT:

A daily oceanic climatology to estimate upper ocean thermal structure was developed for application year-round in the North Atlantic, and North and South Pacific Ocean basins. The Systematically Merged Atlantic Regional Temperature and Salinity (SMARTS) Climatology, the Systematically merged Pacific Ocean Regional Temperature and Salinity (SPORTS) Climatology, and the South Pacific Ocean Climatology (SPOC) blend temperature and salinity fields from the World Ocean Atlas and Generalized Digital Environmental Model at 1/4º resolution for use in a two and half layer model to project sea surface height anomalies (SSHA) into the vertical. This higher resolution approach better resolves features in the Gulf of Mexico (GOM), including the Loop Current (LC) and eddy shedding field, than the coarser 1/2º products of previous studies. Daily mean isotherm depths of the 20ºC (D20) and 26ºC (D26), reduced gravity, and mixed layer depth (MLD) were extracted from the climatology and provide the physical parameters needed for the projection of SSHAs into the vertical. The algorithm for estimation of ocean temperature structure was advanced by an improved characterization of the reduced gravity term and an updated objective analysis scheme.

Using SMARTS, SPORTS and SPOC with satellite-derived SSHA and SST fields, daily values of D20, D26, MLD, and Ocean Heat Content (OHC) were calculated from 1998 to 2014 using a two and a half layer model approach. OHC is an important scalar when determining the ocean's impact on tropical cyclone intensification, as OHC can predict sea surface temperature cooling during hurricane passage, controlling the magnitude of air-sea enthalpy fluxes. Airborne and ship-deployed eXpendable BathyThermographs (XBT), long-term moorings, and Argo profiling floats provided the *in-situ* data necessary to assess SMARTS and SPORTS estimates of isotherm depths and OHC. Based on over 520,000 temperature profiles of *in-situ* data from 1998 to 2014, a clear, direct relationship emerged from the detailed analysis between satellite-derived and *in-situ* measurements of isotherm depths and OHC. The SMARTS, SPORTS and SPOC climatologies significantly improved upper ocean estimates of the thermal structure and OHC.

This improved OHC product was transitioned to NOAA NESDIS as described in this ATBD. Daily fields are generated that includes position, SSHA and error estimates from the objective mapping technique, SST, D20, D26, MLD, and OHC. The successful implementation and use of the product requires data from at least two altimeters and the daily SSHA updates from the U.S Navy ALPS system are sent to the NOAA NESDIS DDS. The product fields will be evaluated monthly when thermal structure data from various platforms become available such as Argo floats, XBT transects, mooring measurements, and airborne profiling from NOAA research aircraft. The software also runs on computers at University of Miami's Rosenstiel School of Marine and Atmospheric Science so the products are accessible for experimental planning and research.

1. INTRODUCTION

1.1 Product Description

Ocean heat content (OHC) is a measure of the integrated vertical temperature from the 26ºC isotherm depth to the sea surface where the temperature is the surface boundary condition (e.g., area under the curve) as shown in Figure 1-1. OHC can be determined from ocean thermal profiles or from satellite derived estimations. An algorithm that generates a set of satellite derived OHC products has been running in development mode for more than 20 years at the NHC and University of Miami's Rosenstiel School of Marine and Atmospheric Science (RSMAS). The algorithm is based on a 2.5-layer reduced gravity ocean model which uses a blended daily ocean climatology of mean isotherm depths and reduced gravities, objectively analysed sea surface height anomaly fields (SSHA) from available altimeter missions (e.g., Jason 1, 2, 3, Envisat, SARAL, Cryosat-2), and satellite sea surface temperatures (SST) from Remote Sensing System's Optimally Interpolated SST and NESDIS GEO-POLAR Blended SST Analysis (Harris and Maturi, 2012) to produce isotherm depths of the 20º and 26º (D20, D26), mixed layer depth (MLD), and OHC. The software is efficient in that additional satellite data such as another set of altimeter-derived SSHA tracks can be easily ingested into the calculation.

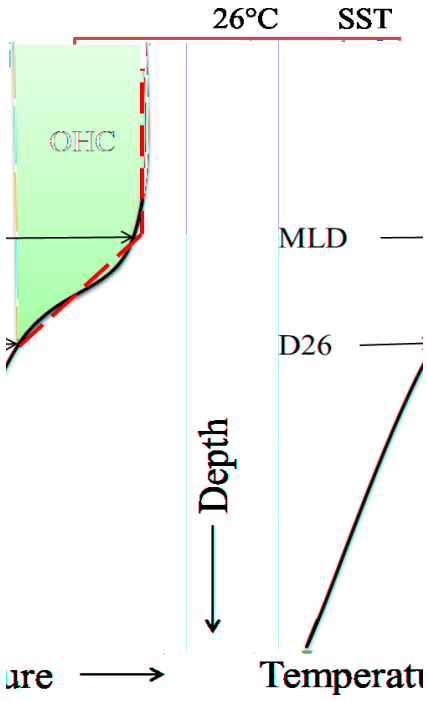

Figure 1-1: Schematic of OHC calculation. The red shading shows the true OHC by integrating the black temperature profile. The dashed blue line shows the approximated temperature profile of the upper ocean.

A high-resolution (0.25° × 0.25°) daily OHC analysis based on this general approach was completed for the North Atlantic and North and South Pacific Ocean basins. The new climatologies, the Systematically Merged Atlantic Regional Temperature and Salinity (SMARTS: Meyers *et al.*, 2014), the Systematically merged Pacific Ocean Temperature and Salinity (SPORTS: McCaskill *et al.*, 2016) and the South Pacific Ocean Climatology (SPOC), are based on a weighted blending of the Navy's Generalized Digital Environmental Model (GDEM: Teague *et al.,* 1990) and the Levitus World Ocean Atlas (WOA). These new daily climatologies provide a higher resolution depiction of the actual OHC for not only hurricane intensity forecasts for the Statistical Hurricane Intensity Forecast Scheme (SHIPS: DeMaria *et al.,* 2005) but also for long-term climate studies and coral reef related research. An important aspect of this project is to provide detailed evaluations of satellite derived fields to *in-situ* data from Argo floats, satellite-tracked drifters, XBT transects, long-term mooring measurements in the equatorial Atlantic and Pacific and dedicated AXBT measurements from NOAA's research aircraft in support of the Hurricane Field Program including those from Deep Water Horizon (DWH) research flights (Shay *et al.,* 2011, Jaimes and Shay, 2015). This work follows recently published approach in the Eastern Pacific and North Atlantic Ocean basins using a revised, blended climatology (Shay and Brewster, 2010; Meyers *et al*., 2014). Such analyses provide biases between the *in-situ* measurements and the fields and products from the satellite-based sensors.

1.2 Product Requirements

The OHC product requires a high resolution SST product for the surface boundary condition of the reduced gravity model. A minimum of two (best practices would be at least three) sets of SSHA tracks from altimetry missions should be used to resolve the oceanic mesoscale variability. Latency of ~36 hours is due to receipt and processing of the SSHAs (e.g., objective mapping). Timeliness is a critical element given that altimetry missions have different repeat cycles owing to their polar orbiting nature with ascending and descending tracks. If an outage extends more than 1 week, the resultant SSHA field will not necessarily be accurate and of limited use particularly for use in hurricane forecast models.

1.3 Satellite Instrument Description

Satellite radar altimeters measure sea surface height along repeated tracks. These polar-orbiting satellites repeat their exact paths on a 10, 17, 29 or 35-day basis depending on mission requirements (Cheney *et al.*, 2002). From 1998 onward, all SSHA fields from radar altimeters over the North Atlantic and North and South Pacific Ocean basins were acquired for this study. Our research studies have shown that at least two active satellites are required for accurate mesoscale applications of altimetry data in determining OHC useful for forecasting hurricane intensity (Mainelli *et al*., 2008; Meyers, 2011). Typically, two or more altimeters were operational at any given time (Table 1-1). Altimetry data were acquired from Naval Oceanographic Office and SSHAs were determined using a background mean SSH from the Collecte Localisation Satellites' Combined Mean Dynamic Topography 2001 (Lillibridge *et al.,* 2011).

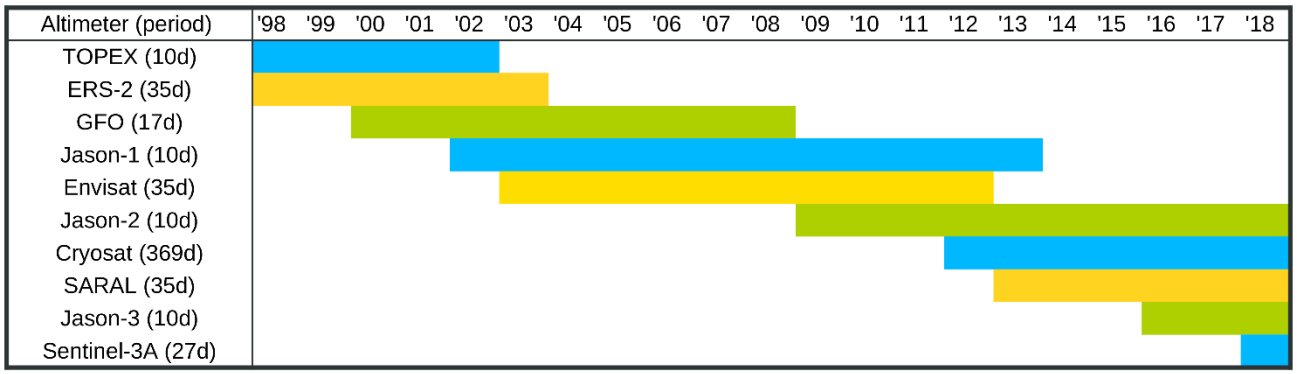

Table 1-1: Summary of altimeters with their respective repeat track cycles in parentheses used in developing the SMARTS, SPORTS, and SPOC systems in generating daily isotherm depths and OHC.

2. ALGORITHM DESCRIPTION

2.1 Processing Outline

The daily real-time OHC processing takes several steps: acquiring the input data, objectively analyzing the SSHA, calculating OHC using the 2.5-layer model, and creating ASCII and netCDF output files of the products (Figure 2-1). The GEO-POLAR blended SST product (Harris and Maturi, 2012) and the altimetry SSHA data files are served to the Data Distribution Service (DDS) each day. Once the retrieval program picks up the data on the DDS (which includes any updates to the data files), the OHC program is started. The software first checks to ensure completeness of the files of SST and SSHA fields. Currently, the SST HDF file is subsampled from 5 km to 0.25° resolution, because the oceanic climatologies, SMARTS, SPORTS, and SPOC are at 0.25° resolution. Thus, all data fields must be at that resolution for internal consistency in the OHC software. Altimetry derived SSHA fields are prepared as ASCII files to be objectively analyzed and mapped using the Mariano and Brown (1992) technique described below. Once this step is completed, the SSHA fields are input into a reduced gravity model and combined with SMARTS, SPORTS, or SPOC to determine the isotherm depths of the 20°C and 26°C water as well as inferring an oceanic mixed layer depth (MLD). The approach then uses the depth of the 26°C isotherm, MLD and SST to estimate the OHC at each grid point over the basin. Lastly, the software produces two output files, an ASCII file and a self-describing netCDF file with all of the products from the OHC processing.

In addition, software will evaluate the data product with Argo floats, XBT transects, long term moorings and AXBTs deployed from research aircraft to evaluate satellite derived fields of isotherm depths, MLD and OHC to refine the uncertainty limits and error bars. This is an important feature of this product because during the hurricane season, the SHIPS model uses OHC to forecast hurricane intensity (DeMaria *et al*., 2005; Mainelli *et al*., 2008; Meyers *et al.* 2014).

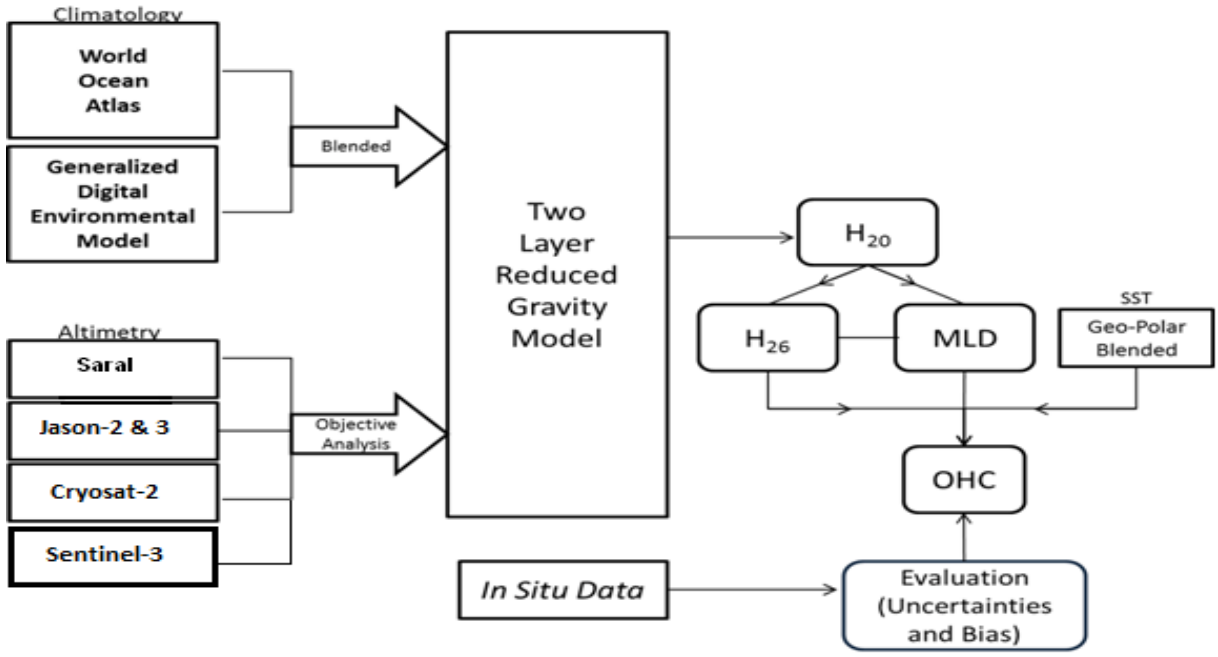

Figure 2-1: Flow diagram of the inputs to the reduced gravity model including the objectively analyzed SSHA from various radar altimeters to estimate the depth of the 20°C isotherm which is then used to determine the depth of the 26°C isotherm and MLD and the GEO-POLAR SST to calculate OHC. *In-situ* data includes temperature profiles from Argo floats, XBT transects, AXBTs deployed from research aircraft, PIRATA moorings in the North Atlantic Ocean Basin and TAO/TRITON moorings in the Pacific Ocean Basin.

2.2 Algorithm Input

The primary satellite data input to this algorithm are: 1) sea surface height anomaly (SSHA); and, 2) sea surface temperatures (SST) from the GEO-POLAR Blended (Harris and Maturi, 2012) product at NESDIS. These data are used in a two and half layer reduced gravity model. Currently, the algorithm uses Jason-2 and SARAL Cryosat-2 data and now includes Jason-3 and Sentinel-3A data. In an evaluation of the products of isotherm depths, mixed layer depth and OHC, the approach uses Argo float profiling floats, XBT transects, moorings such as PIRATA in the equatorial Atlantic Ocean and TAO/TRITON in the equatorial Pacific Ocean, and airborne expendables deployed from NOAA research aircraft including pre-hurricane surveys. These evaluations will be conducted monthly when enough in-situ data become available.

2.3 Theoretical Description

2.3.1 Physical Description

The underlying approach assumes that the ocean can be described as a two-layer fluid with an oceanic mixed layer on top of the upper-most layer. That is, SSHA represent the changes in thermocline depth (e.g. 20^{o}C) based on thermal expansion of sea water. In this context, we infer depths of the 26^{o}C isotherm in the upper layer assuming any thermal changes in the upper ocean layer are compensated by corresponding salinity changes. The two-layer model is considered a crude approach to approximating the upper ocean thermal structure when compared to full 3-D ocean models, but models in use today, such as HYCOM have many assumptions and implications for the various ocean parameterization schemes (Halliwell *et al.,* 2008; 2011). The temperature and salinity relationships (T/S) relationships in the North Atlantic Ocean basin suggest that the depth of the 20^{o}C isotherm is a reasonable proxy for this assumption. Even in the Gulf of Mexico, the subtropical water and Gulf Common water characteristics begin to converge at this isotherm depth (see Section 3 below).

2.3.2 Mathematical Description

Each individual climatology, WOA and GDEM, provided temperature and salinity profiles at each latitude and longitude in its resolution. Each temperature profile was interpolated to a 2-meter increment using a cubic interpolation scheme to maintain a realistic profile at depths where data were less dense. The profiles were interpolated from 2 m, to avoid artificially high ocean skin temperatures, down to the deepest observation. The depths of the 20 and 26°C isotherm were extracted from the profile by linearly interpolating between the two depths surrounding the isotherm of interest of the interpolated profile. The MLD was determined by finding the deepest point of the interpolated profile which is within 0.5°C of the temperature at 2 m. This threshold temperature was chosen following Monterey and Levitus (1997) and because it was outside the precision of the instrumentation. Strictly using a temperature difference from a near surface value was preferred to using a temperature gradient threshold due to the large spatial variability of the structure of the thermocline (de Boyer Montegut *et al.,* 2004). Temperature inversions were not of concern because these typically occur in polar regions, outside of the domain of this study.

Each individual climatology's performance in calculating ocean thermal structure was expected to vary spatially and temporally due to implicit errors in the climatology. In all three basins, the 2001 version of the WOA climatology was investigated and used in the blending. Version 3.0 of the GDEM climatology was used for blending in the North Atlantic, while Version 2.1 of GDEM was used in the North and South Pacific. A different version of GDEM was used in the Pacific basins based on comparisons of thermal structure with in-situ temperatures, similarly seen in Shay and Brewster (2010). Attempts to divide the North Atlantic and Pacific basins into broad analysis regions resulted in minimal differences between skill of the GDEM and WOA climatologies. Instead, the basins were divided into 5°x5° boxes in which blending weights were to be determined for each box. Along borders between two regions, a 2° linear transitional region to smooth the weighting map was used to avoid abrupt borders. The 2° buffer zone was larger than the Rossby radius of deformation (e.g., ~1° in the GOM) to avoid gross distortion of features as they translated through transitional zones.

Weights were determined for the northern hemisphere hurricane season (June 1 – November 30) and off-season (December 1 – May 31) and for the southern hemisphere hurricane season (November 1 – April 30) and off-season (May 1 – October 31). Seasonality of GDEM and WOA necessitated weighting schemes for different times of the year. Local RMSD of each individual climatology determined the blending weights for the SMARTS, SPORTS, and SPOC climatologies. This parameter was selected because it best quantified the predictive strength of the individual climatologies. For each 5° box, the weights of GDEM and WOA were determined based on the relative magnitudes of RMSD following

$$Climatology = \frac{GDEM \cdot RMSD_{WOA}^2 + WOA \cdot RMSD_{GDEM}^2}{RMSD_{WOA}^2 + RMSD_{GDEM}^2}$$

In regions with fewer than 50 observations, WOA and GDEM were weighted evenly due to insufficient sample size. As part of this research effort, regional coherence of the weighting parameters showed both local strengths and weaknesses in GDEM and WOA.

The weighting maps resulting from RMSD analysis depicted the locations where either GDEM or WOA were better suited for ocean thermal structure calculation. The D20 weighting map was created first, considering the new D20 calculations were needed for estimations of D26, MLD, and OHC. The D20 weighting map was also used for the blended climatology of densities for the upper and lower layer in the two-layer model.

For the North Atlantic hurricane season, the two-layer model calculated D20 better using the GDEM climatology in the GOM and most of the LC regime (Figure 2-2). In fact, GDEM also outperformed WOA along the U.S. coastline, being slightly better in the colder waters north of where the Gulf Stream (GS) separates from the coastline near Cape Hatteras, North Carolina. In general, the subtropical waveguide was dominated by GDEM, particularly along the African coast. The southern extent Caribbean Sea and the center of the subtropical gyre tended to be better predicted using WOA. In this regard, a blending of these two climatologies was warranted for SMARTS.

Outside of the hurricane season, observations were more sparse and the ventilation of D26 at the surface moves southward during the winter and spring months. Again, GDEM vastly outperformed WOA in the equatorial wave guide. WOA predicted D20 better near the Caribbean Islands and in the western GOM whereas GDEM only slightly improved calculations along the mid-Atlantic and western Florida coasts. Once the weighting maps of D20 were calculated, $\overline{\mathbf{D20}}$ (mean depth of the 20°C isotherm discussed below) was recalculated for the entire basin. Daily values of D26 and MLD were then determined based on the ratio between GDEM and WOA climatological values of these parameters and the SMARTS climatological value of D20. Following this approach, analysis showed GDEM typically performed better in the Caribbean Sea and the western GOM, although neither climatology showed marked improvements in the GOM eddy shedding region (not shown). Elsewhere in the Atlantic Ocean basin, WOA typically outperformed GDEM except in isolated locations. Generally, WOA was better for D26 calculations outside of the hurricane season.

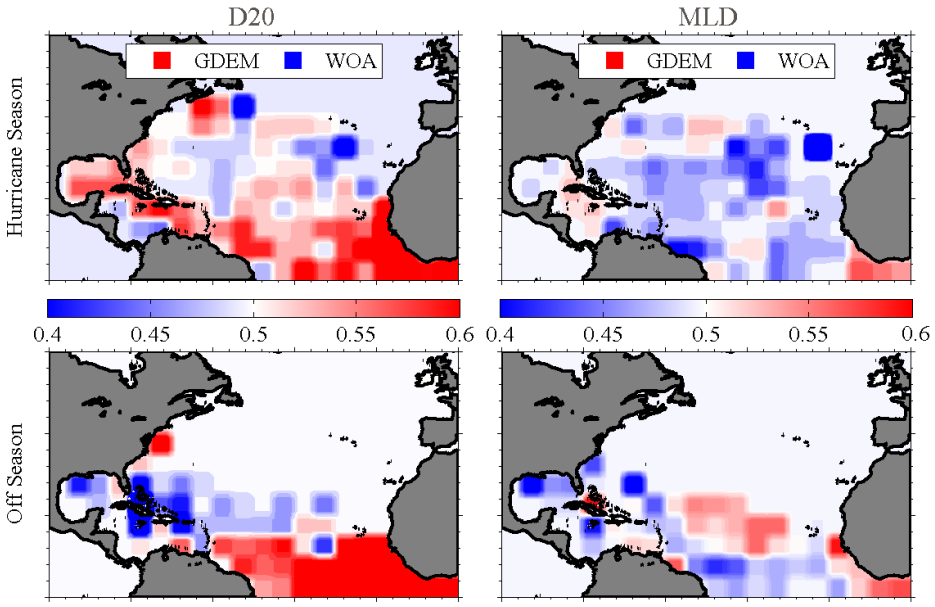

Figure 2-2: Weighting maps for D20 (left) and MLD (right) used to create the SMARTS climatology for the hurricane season (top row) and outside of the hurricane season (bottom row).

Weighting maps for MLD were more erratic, although some regional coherence existed in the basins. In the GOM during hurricane season, neither climatology stood out in particular, although GDEM was slightly more accurate in the Caribbean Sea and the LC. Elsewhere, WOA was typically more accurate other than a few locations where GDEM held a slight advantage. Outside of the hurricane season, WOA was better for MLD calculations in the GOM and the western equatorial Atlantic Ocean. GDEM marginally improved satellite MLD calculations off the northern South American and African coasts, as well as in the central North Atlantic Ocean basin. Using these weighting maps with climatological values for D20, D26, and MLD, the SMARTS Climatology was created. Daily values of D20, D26, MLD, and OHC were recalculated using satellite altimetry and the new climatology, such that it could be compared to results from analyses utilizing the Mainelli (2000) climatology and determine if a relative or absolute weighting method was preferable.

In the North Pacific Ocean basin, the weighting maps resulting from RMSD analysis also depicted the locations where either GDEM or WOA were better suited for ocean thermal structure calculation. As in SMARTS, the D20 weighting map was created first, considering the new D20 calculations were needed for estimations of D26, MLD, and OHC. The D20 weighting map was also used for the blended climatology of densities for the upper and lower layer in the two-layer model. For the TC season, the two-layer model calculated D20 better using the WOA climatology in the (Figure 2-3) over most of the basin except for the western and eastern Pacific warm pools and the South China Sea. The eddy rich regimes in the western and eastern Pacific are captured by GDEM. During the off-season, WOA dominates over most of the basin except in the equatorial eastern Pacific Ocean and the South China

Sea. The predominance of the GDEM signals is much clearer during the TC season than in the off season. A similar pattern emerged for the MLD in both the TC season and the off season for the North Pacific Ocean basin. The WOA climatology for the MLD outperformed GDEM even in the eddy rich domain of the western North Pacific Ocean Basin. However, in the South China Sea and the Eastern Pacific Ocean basin, GDEM outperformed the WOA climatology.

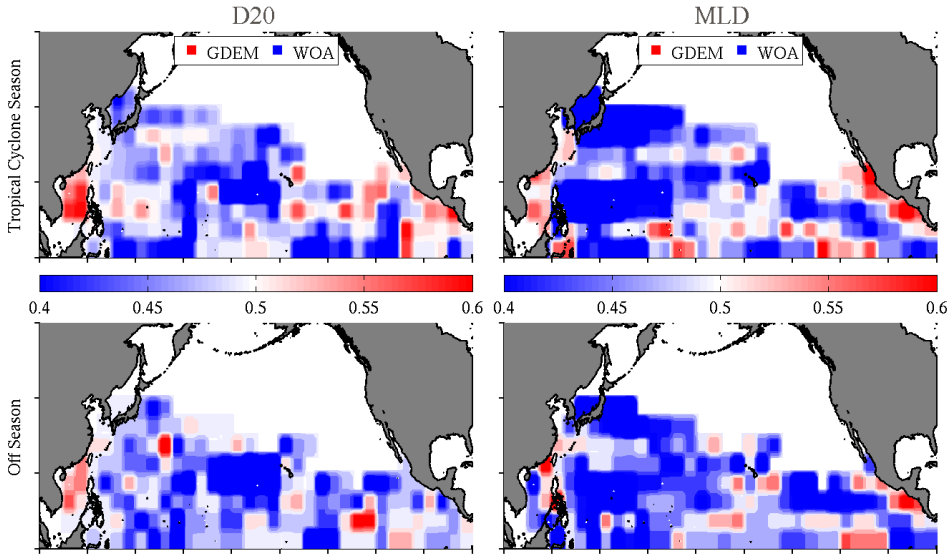

Figure 2-3: Same as Figure 2-2 used in the SPORTS climatology.

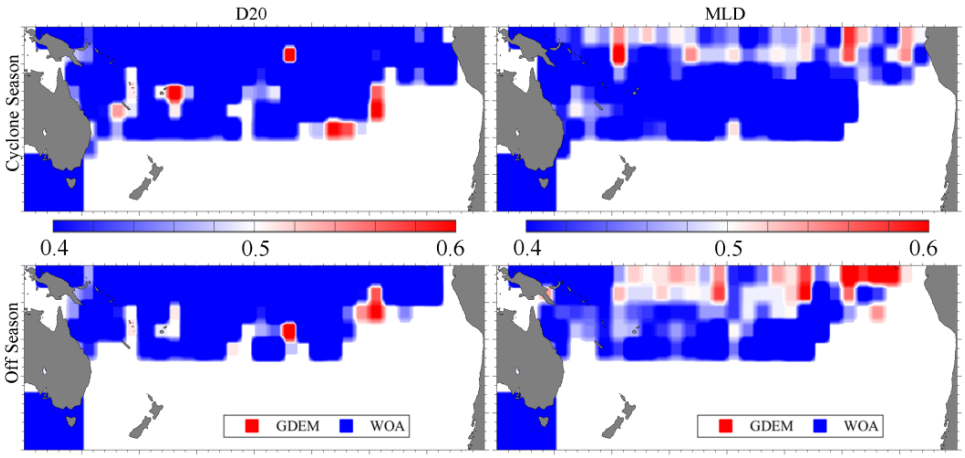

Figure 2-4: Same as Figure 2-2 used in the SPOC climatology.

The D20 weighting maps for the South Pacific (Figure 2-4) determined whether WOA or GDEM correlated better with the *in-situ* RMSD comparisons. Over most of the domain, the WOA climatology dominated the D20 weighting over the GDEM climatology in both the cyclone season and off season

for D20. GDEM was more accurate in a region on the eastern side of the domain and several small areas in the center of the basin and near the islands of Fiji, New Caledonia, and Vanuatu. The area south of Australia uses the absolute value of WOA D20, because the GDEM climatology does not cover that region. In the South Pacific, MLD weighting is more variable. GDEM is weighted higher in the equatorial region, particularly towards the South American continent. South of the tropics, WOA dominates the weighting. The off season weighting is a little more variable than the cyclone season. Again, the area south of Australia uses the absolute value of WOA for MLD, because the GDEM climatology does not cover that region.

To justify the use of these climatologies, the resulting blended fields must depict realistic fields of these spatially varying variables. When using the absolute blending technique (not shown), sharp transitions between the GDEM and WOA climatologies created an unrealistic field. Visual inspection of a sample of climatological fields based on the absolute blending scheme showed no evidence of transitional areas. *Therefore, the relative blending scheme was used to create the realistic fields for all parameters needed for the approach model for SMARTS, SPORTS, and SPOC.*

Following Leipper and Volgenau (1972), OHC is calculated from the surface to D26,

$$\mathrm{OHC_{Obs}} = \int_{D26}^{Sfc} c_P \rho_{T,S} (T - 26°C) dz.$$

Density was calculated at every depth using a 4th order polynomial (Miller and Poisson 1981) dependent on temperature and an assumed salinity of 35 psu. The specific heat of water, c_p, was taken as 4200 $J \cdot kg^{-1} \cdot C^{-1}$.

GDEM and WOA climatologies provided the 4-dimensional data needed to construct the climatology necessary for the implementation of the two-layer model for calculation of ocean thermal structure. Extracted profiles of temperature and salinity were interpolated to a 1-m resolution using a cubic interpolation scheme. An iterative process then identified the depth of the 20 and 26°C isotherms and applied a linear interpolation between the two points surrounding the isotherm depth to approximate the appropriate depth. MLD was defined as the depth where the temperature deviates from the SST by a magnitude of 0.5°C. The 2.5-layer model depended on a density difference between upper (ρ_1) and lower (ρ_2) layers. The interface between layers was assumed to be the 20°C isotherm because it was typically within the thermocline. Density was calculated at each level of the climatology and the density of each layer (ρ_1 and ρ_2) was estimated as the arithmetic mean of the layer. From the values of density, the reduced gravity, g′, was calculated by

$$g' = g \frac{\rho_2 - \rho_1}{\rho_2} \quad ,$$

where g us the acceleration due to gravity (9.81 $m \cdot s^{-2}$). If g' was less than 0.2 $m \cdot s^{-2}$, g′ was set to 0.2 $m \cdot s^{-2}$ to avoid unrealistic values when applied in the two-layer model. A 15-day running mean applied to the monthly climatologies ensured smoother monthly transitions (Figure 2-6). This blending technique created a daily climatology which can be used as a background for altimetry calculations.

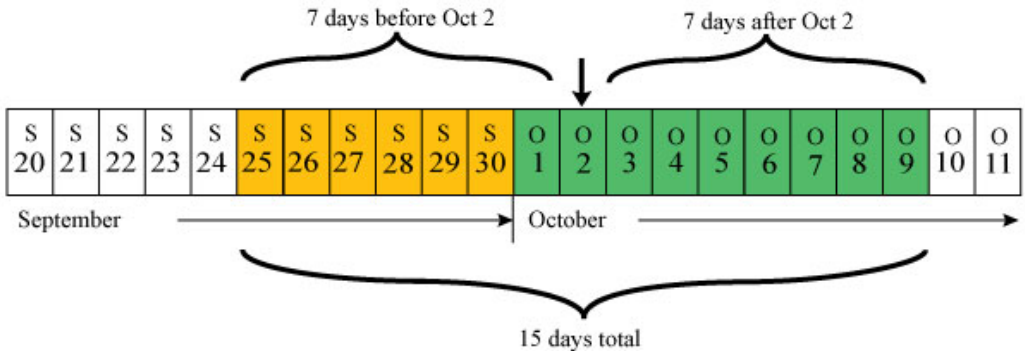

Figure 2-5: A 15-day running mean was used to create the 'daily' climatology. For example, to create the October 2nd climatology, the September climatology was weighted 6/15 and the October climatology is weighted 9/15.

SSHA data were unevenly spaced over the basin, which necessitated an Objective Analysis (OA) scheme to interpolate data to a regular grid. The parameter matrix algorithm of Mariano and Brown (1992) grids non-stationary fields using time-dependent correlation functions. SSHA data from 5 days before and 5 days after the date of interest were used to ensure basin-wide coverage by at least the 10-day repeat track altimeters. Parameters for spatial and temporal correlation scales followed Mainelli (2000) and are presented in Table 2-1. The SSHA field was assumed to have uniform variance and measurement noise was uncorrelated. The OA was performed locally point-by-point, using 20 influential data points determined by the correlation model from Mariano and Brown (1992) which accounts for phase speeds, zero-crossing scales, and spatial and temporal decay scales.

Operational Mode	Dynamic Height
Roughness Parameter	1.1
Tension	0.9
Spline	Bicubic
Influential points	20
Zero crossing scale	1.8°
e-folding scale	1.2°
Temporal decay scale	20 days
Confidence level	0.95

Table 2-1: Key parameters used in the OA following Mariano and Brown (1992).

Previous OA assumed a uniform drift velocity over the North Atlantic and North and South Pacific Basins to the west-southwest (0.03 °/day westward, 0.01 °/day southward). Drift velocities vary spatially with latitude and along bathymetric features (Chelton and Schlax, 1996). To assess the spatial variability of feature drift velocity, North Atlantic SSHAs from 2005-2007 were OAed without any

drift velocity correction (Figure 2-7). Three years of OA SSHA fields were plotted in Hovmöller diagrams with a north-south and east-west cross-section for all 10°x10° grid boxes. If the SSHA showed clear trends, the drift velocity for that grid was determined by taking the average speed of three subjectively chosen trend lines. The entire SSHA dataset was reanalyzed to make adjustments using these estimated drift velocities. Similar results were found in the western North Pacific Ocean basin in the eddy rich zone at about 25ºN from 2002-2004, and in the central South Pacific Ocean basin at 25º S from 2002-2004. Although in some areas, eddy variability may be much slower that these rates due to the underlying ocean dynamics.

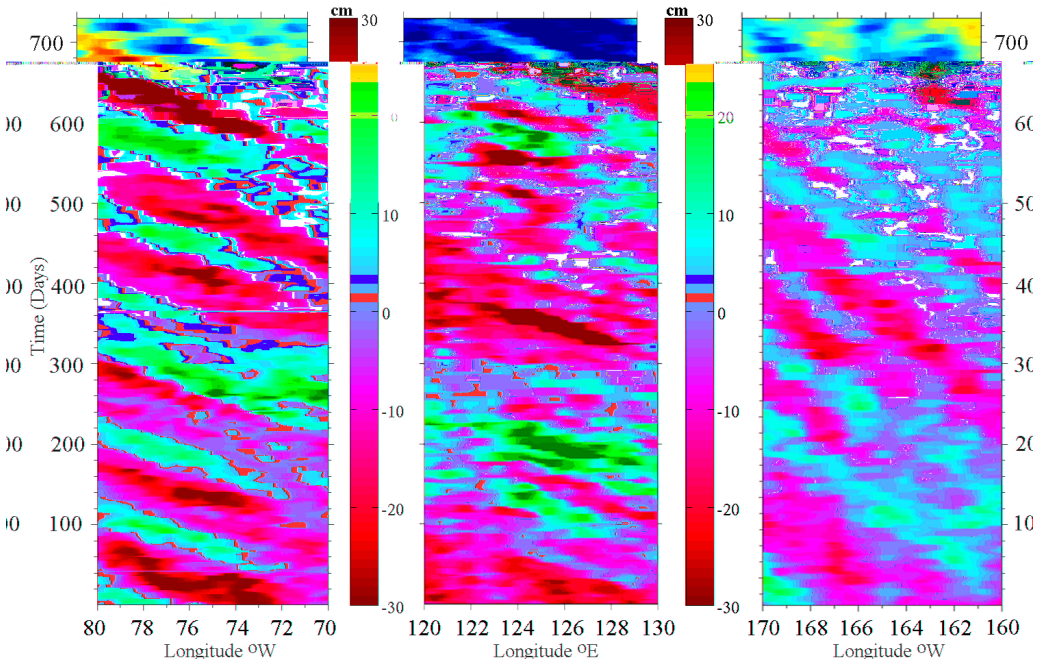

Figure 2-6: Hovmöller of SSHA at 15°N in Caribbean Sea (left), at 25ºN in the Western North Pacific Ocean Basins (middle), and at 25ºS in the South Pacific for two years. Drift velocities are on the order of 0.1°/day compared to previous estimates of as much as of 0.3°/day.

A reduced-gravity model adjusted the climatological values of D20, D26, and MLD in relation to SSHA. In a two-layer model, changes in SSH reflect changes in the depth of the interface between layers. If the SSHA was positive (negative), then the upper (lower) layer was thicker (thinner) and the interface depth was deeper (shallower). The inferred depth of the 20°C isotherm (D20′) is a function of the reduced gravity, the climatological depth of the 20°C isotherm ($\overline{D20}$) and the SSHA, η′.

$$D20' = \overline{D20} + \frac{\rho_2}{\rho_2 - \rho_1}\eta' \quad .$$

A uniform stretching or shrinking of the upper layer was assumed in order to calculate the depth of the 26°C isotherm (D26′) and MLD′. Therefore, the displacement of D26′ and MLD′ was determined by the climatological ratio between the variable of interest and $\overline{\mathrm{D20}}$.

$$\mathrm{D26'} = \frac{\overline{\mathrm{D26}}}{\overline{\mathrm{D20}}}\mathrm{D20'},$$

$$\mathrm{MLD'} = \frac{\overline{\mathrm{MLD}}}{\overline{\mathrm{D20}}}\mathrm{D20'} \quad .$$

Calculations of D20′, D26′, and MLD′ were performed at every grid point in the ocean domain with depths greater than 100 m. If the depth of the calculated isotherm was deeper than the bathymetry, then the isotherm depth was set to be the depth of the ocean bottom. OHC was calculated by adjusting the OHC expression assuming a temperature profile with a homogeneous mixed layer with satellite SSTs and a constant temperature gradient from the base of the mixed layer to D26′

$$\mathrm{OHC'} = \frac{1}{2}\rho_1 c_P(\mathrm{D26'} + \mathrm{MLD})(\mathrm{SST} - 26°\mathrm{C}) \,.$$

The estimation of OHC′ is presented graphically in Figure 1-1. Previous studies assumed a climatological mixed layer (Shay and Brewster, 2010). Meyers *et al.* (2014) compared MLD′ to in-situ MLD values to determine if equation (7) is a valid technique for estimating MLD for OHC estimations. In-situ data (D20, D26, OHC, MLD) were compared to the satellite-derived data at the nearest corresponding grid point. To account for errors in the OA, only profiles with corresponding OA errors of less than 0.5 were compared. This method of calculating ocean thermal structure was confirmed to be practical using the GDEM climatology.

2.4 Algorithm Output

Output data products from the OHC software consists of two files in ASCII and NETCDF where the output is defined on a 0.25° grid. For the daily files, the fields are latitude, longitude, sea surface temperature (°C), sea surface height anomaly (cm), mapping error of the SHA field from the objective analysis scheme, 20°C and 26°C isotherm depths, ocean mixed layer depths (m) and OHC ($kJ \cdot cm^{-2}$).

2.5 Performance Estimates

2.5.1 Data Description

From 1998 to 2014, detailed tests were conducted by comparing the satellite-derived products to *in-situ* data sets from Argo floats (see: http://www.argo.ucsd.edu or http://argo.jcommops.org), XBT transects (see https://www.nodc.noaa.gov/GTSPP/), PIRATA and TAO/TRITON moorings, and aircraft expendables (AXBT/AXCTD) including the Deep Water Horizon measurements from May through July 2010 (Shay *et al*., 2011) and EPIC from 2001(Raymond *et al.*, 2004; Shay and Brewster,

2010). In addition, test data sets also included examining the sensitivity of the products on various SST products. These types of tests will also be conducted during operations to maintain the system in producing the highest quality product possible.

2.5.2 Sensor Effects and Errors

The SSHA data from the various altimeters are processed through the ALPS system at NAVO then sent to the DDS system at NESDIS. In addition to orbit corrections, the resultant fields have been corrected for ionospheric processes, electromagnetic biases, inverse barometric effects and wet and dry tropospheric processes (Lillibridge *et al*., 2011). We expect that the resultant SSHA field has an uncertainty of less than a few cm (Cheney *et al*., 2002).

2.6 Practical Considerations

2.6.1 Numerical Computation Considerations

The algorithm includes an objective mapping and blending technique (Mariano and Brown, 1992) that was tested on different data sets including basin scale SSTs. Any updates to that code would be done in a research environment at the University of Miami to assess its impact on the OHC operations at NESDIS.

2.6.2 Programming and Procedural Considerations

Codes are straightforward and documented to show the progression of the steps as shown in the flow diagram (Fig 2-1). Any major changes will have to be thoroughly tested in a research mode (includes (new *in-situ* data that may become available in the future) before recommending a change to the operational software.

2.6.3 Quality Assessment and Diagnostics

The products are evaluated once a month with detailed comparisons to available *in-situ* data as discussed above. This includes least squares fits and regression analyses to assess any problems with the input data since the climatology is relatively steady.

2.6.4 OHC Data Quality Flags

Referencing values of OHC=0.0 as invalid data should be avoided when defining flags for invalid data—the 0.0 values are intentional to suggest that OHC is still valid but is zero. Data values of OHC=0.0 physically mean that upper-ocean waters (and SSTs) are cooler than 26 ºC, which is common in winter and at higher latitudes—or in the wake of many intense storms. Values of OHC=-999 should overwrite any bad or missing data. An alternative for using -999 as bad or missing data is using NaN (recommended approach).

2.7 Evaluation and Validation

From 1998 to 2014, over 520,000 profiles provided the *in-situ* oceanographic data to evaluate the empirical calculation of D20, D26, MLD, and OHC from the OHC algorithm with SMARTS, SPORTS and SPOC climatologies (Meyers, 2011; Shay *et al.,* 2011; Meyers *et al*., 2014). Over 45,000 profiles over the entire North Atlantic Ocean basin were collected from Lagrangian Argo profilers, ship-borne eXpendable BathyThermographs (XBTs), Airborne eXpendable BathyThermographs (AXBTs), Conductivity, Temperature, and Depth (AXCTDs), and Current Profilers (AXCPs), as well as long-term PIRATA moorings (Servain *et al*., 1998). In the North Pacific Ocean basin over a similar time span (1998-2012), over 267,000 thermal profiles were used in the careful evaluation of the product. As in the Atlantic basin this included floats, XBT transects, process related studies such as the EPIC experiment (Raymond *et al*., 2004; Shay and Brewster, 2010) AXBTs and the long term TAO/TRITON mooring array along the equatorial region essentially spanning from 10^{o}S to 10^{o}N (Croin *et al.,* 2002). Over 210,000 thermal profiles were used in the evaluation of the South Pacific product. As before, this includes Argo floats, XBT transects, and TAO/TRITON moorings.

2.7.1 North Atlantic Ocean

Basin-wide profiles of temperature and salinity are available from the Argo float array (Figure 2-7a). At any given time, approximately 3000 Argo floats are deployed over the world's oceans. The typical sampling mode of a float is to descend to a "parking depth" of 1000m, where it remains for approximately 10 days. Temperature measurements are accurate to ±0.005°C, with depths accurate to ±5m (Carval, 2010). The real-time data product is used because temperature and depth measurements are sufficiently accurate. Nineteen automated quality control checks of the real time data are performed to ensure a realistic profile. These data are valuable in assessing the climatologies because data are collected in all regions of the open Atlantic and Pacific and the floats cover data gaps of the repeat XBT tracks. However, observations are sparse in the GOM because of the short residence time of floats in the LC and geography restricting the profile from completing a full 2000-m profile. XBTs are deployed by vessels of opportunity during cross-basin cruises, creating a "snapshot" of the spatial variability of temperature in the water column (Figure 2-8b). The XBT payload contains a resistor, whose data is transmitted by a fine copper wire back to the ship. The voltages are a measure of the resistance of a conductive material, which is directly related to the environmental temperature surrounding the thermistor. Older XBTs are accurate to approximately ±0.5°C, while newer models are accurate to ±0.2°C (Singer, 1990). Data acquired from XBTs are valuable to diagnose spatial characteristics of ocean thermal structure. Transects provide high resolution data across features of interest, such as the across the GS determine the horizontal variability of temperature in regions large structural gradients. Temporal changes of these features can be diagnosed by examining repeated ship routes.

Ocean observations on synoptic scales and mesoscale can be collected using expendable probes launched from an airborne platform. Airborne expendable bathythermographs (AXBTs), conductivity, temperature, and depth profilers (AXCTDs), and current profilers (AXCPs) are launched by NOAA

WP-3D aircraft during reconnaissance flights (Figure 2-7c). When the profiler is launched by the aircraft, a parachute is deployed to minimize surface impact. Within a minute on the ocean surface, the radio frequency transmitter turns on (known as quieting), within the next 20 to 40 sec, the probe is released from the surface unit where the probe is connected to the unit with thin wire. Data are multiplexed up the wire, and sent to the aircraft via the RF transmitter where the audio signals are received and processed. As with the XBT, the AXBT measures the voltages that are converted to temperatures. Both the AXCTD and AXCP also measures temperature as well as salinity via a conductivity ratio (AXCTD) and currents (AXCP). The fall rates of the AXCTD and AXCP are 2.2 and 4.5 m s^{-1}, respectively. The AXBT fall rate is 1.5 m s^{-1}. A large fraction of the aircraft data were collected during NOAA Hurricane Hunter reconnaissance and research missions prior to, during, or after hurricane passage such as Isidore and Lili in 2002 (Shay and Uhlhorn, 2008); Rita in 2005 (Jaimes and Shay, 2009) and Gustav and Ike in 2008 (Meyers *et al*., 2015). In addition, over 800 profilers were deployed in support of the Deepwater Horizon (DWH) oil spill of 2010 (Shay *et al.,* 2011).

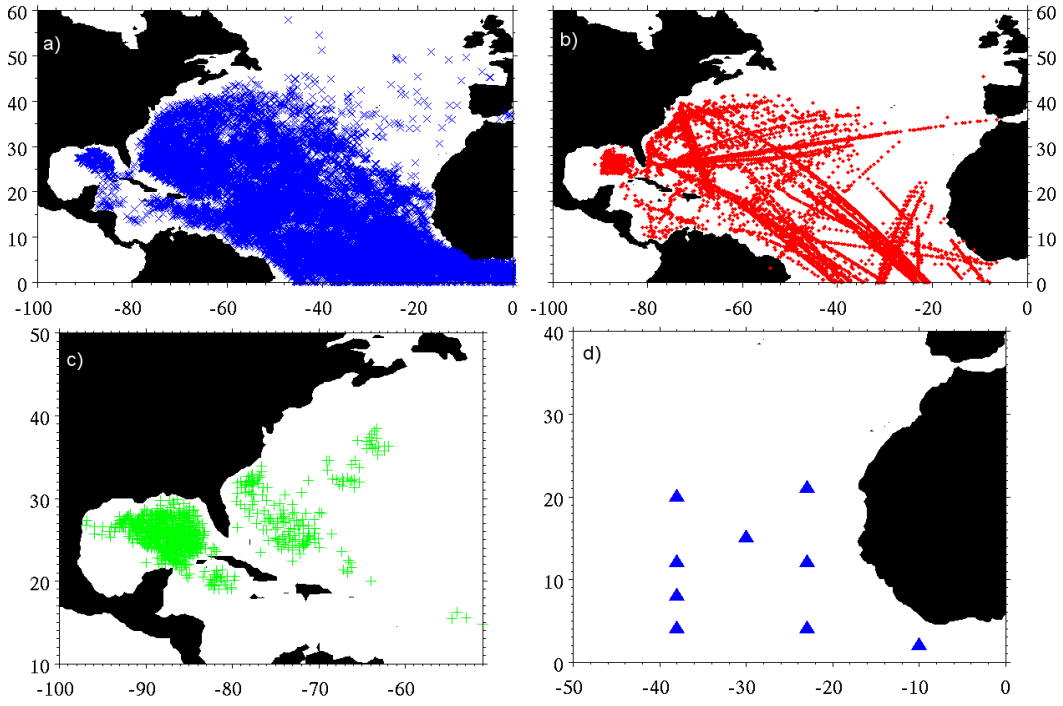

Figure 2-7: Distribution of a) Argo floats, b) XBT transects from research ships and Ships of Opportunity, c) AXBTs, AXCTDs and AXCPs deployed from research aircraft, and d) PIRATA moorings used in the evaluation of SMARTS OHC algorithm.

Raw profiles are passed through a 9-element median filter to remove spikes in the data. The profile is then visually inspected to remove any remaining noise or questionable data. To check for potential gross bias of the data, profiles are compared to surrounding profiles. Noisy profiles are removed from the dataset. Note that temperatures from AXBTs and AXCPs are accurate to ±0.2°C, while AXCTDs

are accurate to ±0.12°C (Johnson, 1995). Comparisons of AXCTD data from the EPIC field program to simultaneous ship-based CTD measurements confirm that AXCTDs are a viable method of acquiring accurate hydrographic data (Shay and Brewster, 2010). That is, airborne oceanography permits sampling of mesoscale and synoptic features at time scales such that the feature does not significantly change over the sampling period. The airborne expendable data fills in a major data gap in the LC and the Gulf of Mexico. Flights typically target regions of high eddy variability and locations of anomalously high or low SSHs from radar altimeters. These data are compared to satellite-derived data to determine if the satellite data resolve large changes in ocean thermal structure after significant wind forcing events.

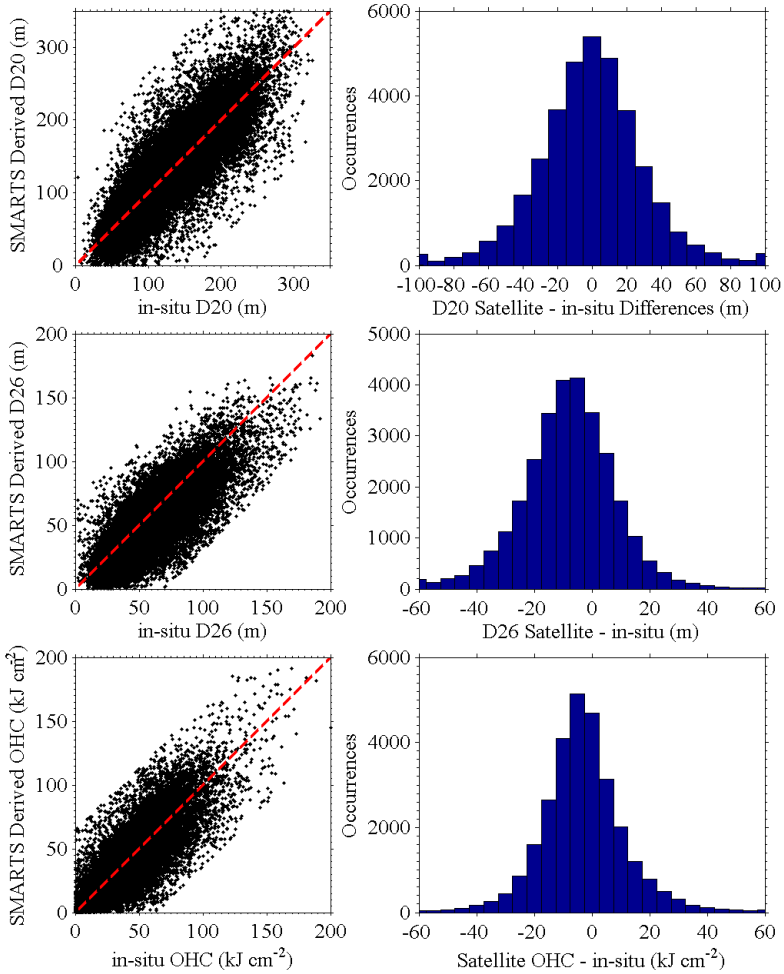

Figure 2-8: Scatterplots (left) of D20 (top), D26 (middle), and OHC (bottom) comparing *in-situ* measurements to values derived by the two-layer model using the SMARTS Climatology. Data points with differences greater than 4 standard deviations from the mean were removed (<0.5% of points). Histograms (right) of errors have bin widths of 10 m, 5 m, and 5 kJ·cm^{-2} for D20, D26, and OHC, respectively.

The Pilot Research Moored Array in the Tropical Atlantic (PIRATA) off the African coast provides temperature data along in the upper ocean (Servain *et al.,* 1998) (Figure 2-7d). Temperature data from the surface to 500 m are measured by a thermistor chain at a vertical resolution of 20 m in the top 140m, and at depths of 180, 300, and 500 m. Daily temperature data accurate to ±0.01°C at the surface and ±0.09°C subsurface are sampled for analysis. When temperature changes of over 5°C occur from the previous day with unrealistic vertical temperature gradients the data are not used in the analysis. Each thermal profile was interpolated to a 2-meter increment using a cubic interpolation scheme to maintain a realistic profile at depths where data were less dense, such as deep in the PIRATA array and at depth for XBTs. The profiles were interpolated from 2 m, to avoid artificially high ocean skin temperatures, down to the deepest observation. The 20 and 26°C isotherm depths were extracted from the profile by interpolating between the two depths surrounding the isotherm of interest of the interpolated profile, which reduces the error in retrieval considerably. Collectively, the *in-situ* profiles provided the necessary data to optimally create and analyze the SMARTS, SPORTS, and SPOC Climatologies.

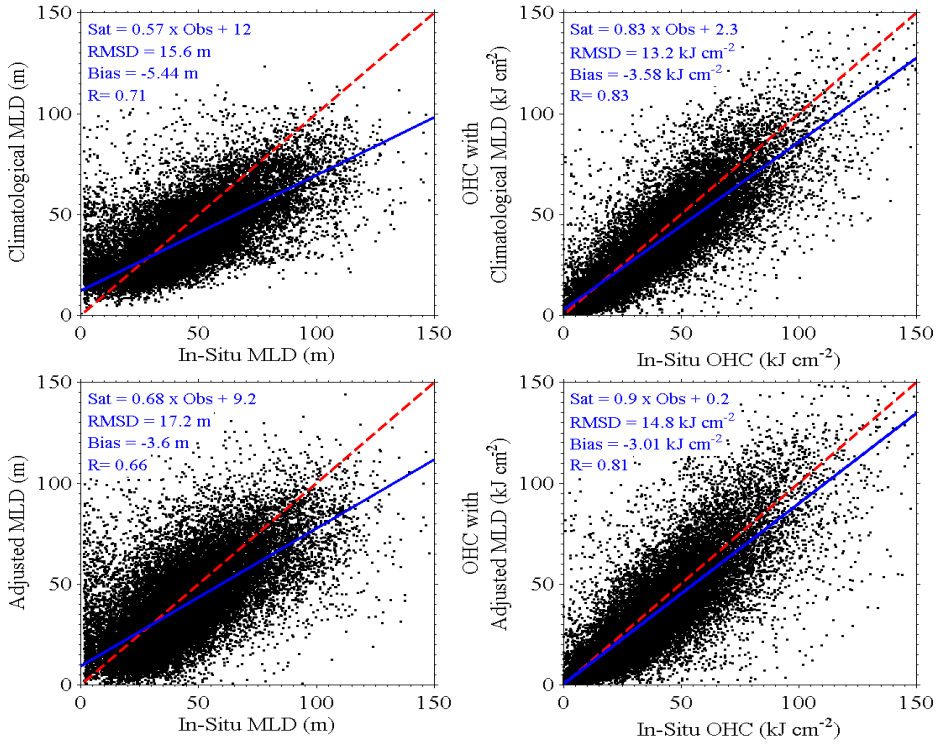

Figure 2-9: Scatterplots of MLD (left) and OHC (right) comparing *in-situ* observations to satellite estimations using climatological MLD (top) and the adjusted MLD (bottom). The red dashed line represents a 1:1 relationship and the linear regression line is solid blue.

Scatterplots comparing *in-situ* values to SMARTS-derived data showed strong correlations, with values typically falling near a slope of unity (Figure 2-8). Histograms of absolute differences between satellite and *in-situ* data showed errors of SMARTS were normally distributed around the mean bias

where 69% of satellite calculations of D20 were within 20 m of the observed value and 89% were within 40 m. The negative bias of D26 was visually noticeable in the histogram as only 65% of D26 SMARTS calculations were within 15 m of the observed value, while 90% were within 30 m. For OHC, 85% of satellite calculations were within 20 $kJ \cdot cm^{-2}$ of observed values. The MLD was determined by finding the deepest point of the interpolated profile which is within 0.5°C of the temperature at 2 m (Fig. 2-9). This threshold temperature was chosen following Monterey and Levitus (1997) and because it was outside the precision of the instrumentation. Strictly using a temperature difference from a near surface value was preferred to using a temperature gradient threshold due to the large spatial variability of the structure of the thermocline (de Boyer Montegut *et al*., 2004). Temperature inversions were not of concern because these typically only occur in polar regions, well outside of the domain of this study. Note the MLD was adjusted using the approach outlined above.

2.7.2 North Pacific Ocean

As shown in Figure 2-10a, Argo float derived thermal profiles were available basin-wide for the North Pacific from 2000-2011. In addition, ship-based expendable bathythermographs (XBT) are acquired through Volunteer Observing System (VOS), Ship of Opportunity Program (SOOP) and on NOAA, UNOLS, and Coast Guard vessels (Figure 2-10b). These data are routinely provided to AOML via a Windows based real-time ship and environmental data acquisition and transmission system. This software creates a series of reports, which describe ship movements that are transmitted in a real-time via the Global Telecommunication System (GTS) to operational data bases to be used by scientists. Specifically, XBT profiles from the ships involved in the SOOP are transmitted to receiving stations onshore via satellite. These data are placed in the GTS and are made publicly available. The global spatial data are available since 1999. Here we accessed data from the website at NOAA AOML and processed the data from the Pacific Ocean basin from 2000- 2011. (See http://www.aoml.noaa.gov/phod/trinanes/SEAS/).

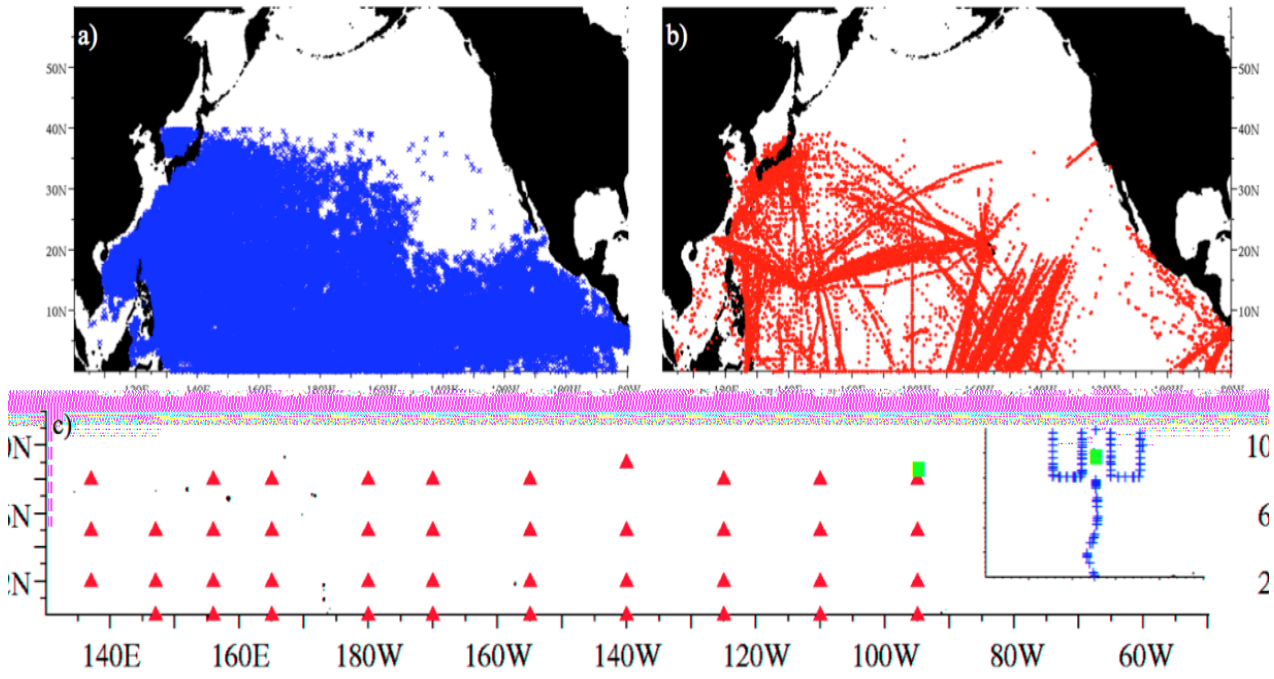

Figure 2-10: Distribution of a) Argo floats, b) XBT transects from research ships and Ships of Opportunity, c) TAO/TRITON moorings with the EPIC 2001 inset showing grids and transects of aircraft expendables deployed from the NOAA WP-3D and the NCAR WC-130J used in the evaluation of OHC algorithm for SPORTS.

The NOAA Tropical Atmosphere Ocean (TAO/TRITON) mooring array used in assessing SPORTS consists of 42 moorings spanning the Tropical Northern Pacific Ocean (Fig 2-10c). Daily sea surface and subsurface temperatures are measured at 10 to 15 different depths in the upper 500m with a concentration of measurements in the first 100m During the EPIC program (Fig 2-11c inset), these TAO/TRITON moorings were enhanced to acquire temperature measurements at 1, 5, 10, 20, 40, 60, 80, 100, 120, 140, 180, 300 and 500 m, and salinity at 1, 5, 10, 20, 40, 80 and 120 m at 8, 10 and 12°N, 95°W (Cronin *et al.* 2002; Raymond *et al.,* 2004). TAO/TRITON temperature structure data from moorings at 95°W, 110°W and 140°W were used to assess the OHC climatology based on satellite sensing. The thermistors making the temperature measures have a resolution of 0.001°C and an accuracy of ± 0.02°C (Freitag *et al.,* 2005). Pacific Marine Environmental Laboratory (PMEL) performs an extensive quality control of the data. Temperature values greater than 99°C and less than -9°C are flagged as missing data. Changes in temperature greater than 5°C and vertical gradients between adjacent sensors are also flagged. Any temperature readings outside 3 standard deviations from the 90-day mean are flagged as well. PMEL also performs a visual inspection of the profile. Data from these moorings were collected daily over a 12-year period from 2000 to 2011.

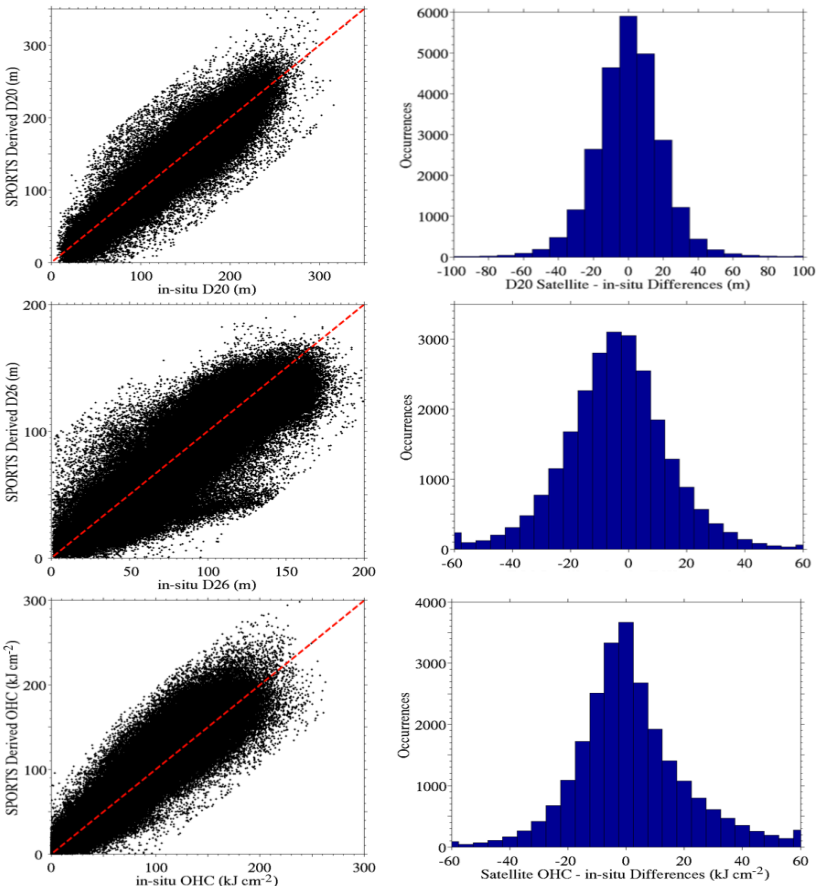

Figure 2-11: Same as Figure 2-8 except for the SPORTS Climatology.

Each temperature profile was interpolated to 1-m resolution using a piecewise cubic Hermite interpolating polynomial from the 1 m depth to 500 m. The 1-m depth was used instead to avoid an artificially high ocean skin temperature. The depth of 20° and 26° isotherms were calculated using a linear interpolation scheme using the two depths around the closest to the desired isotherm. The mixed layer depth (MLD) was defined as the depth at which the temperature was 0.5°C cooler than the 1-m temperature (Monterey and Levitus, 1997).

Argo floats, ship-based expendable bathythermographs (XBTs), EPIC field experiment, and long-term moorings from the Tropical Atmosphere and Ocean (TAO/TRITON) array provided *in-situ* data from 2000-2011 to help assess the World Ocean Atlas 2001 (WOA) and Generalized Digital Environment Model 2.1 (GDEM) climatologies for their use in the SPORTS climatology. GDEM and WOA were then combined with satellite-derived SST and SHA fields from radar altimetry, OHC, MLD, and the 20 and 26^{o}C isotherms were estimated using an the two-layer model from 2000-2011(Mainelli, 2000; Pun *et al.*, 2007; Shay and Brewster, 2010; Meyers *et al.,* 2014).

Shown in Fig. 2-11, a regression analysis was performed over the North Pacific Ocean basin between the *in-situ* and model calculated parameters of OHC, MLD, D20, D26 over the 12-year time period that included approximately 267,000 thermal profiles. The root mean square difference values determined from this analysis will help determine the weights that each climatology were given when creating SPORTS.

2.7.3 South Pacific Ocean

Temperature profiles were acquired from several *in-situ* platforms, Argo floats (Figure 2-12a), XBT transects from research ships and Ships of Opportunity (Figure 2-12b), and TAO/TRITON moorings (Figure 2-12c), spanning the South Pacific Ocean from 1998-2014. Temperatures from different types of platforms were used to capture the temporal and spatial differences inherent in using stationary versus free-roaming instruments.

Argo floats allow for continuous measurement of temperature and salinity in the South Pacific Ocean over many locations. Available from 2000-2014, these data are valuable in assessing SPOC because the Lagrangian nature of the floats allow data collection in all regions of the open ocean and cover data gaps of the repeat XBT tracks and moorings.

The Global Temperature and Salinity Profile Programme (GTSPP) XBT data were available in the South Pacific from 2000-2014. The GTSPP is a joint Intergovernmental Oceanographic Commission and World Meteorological Organization program that maintains a global ocean database of temperature and salinity that are both up-to-date and of the highest quality. Data provided by the GTSPP include all profile data reported through the WMO GTS system. The automated quality control is similar to the tests that the Argo program uses, and the manual component catches failures not detected automatically. Quality reviewing procedures include metadata checks, review of the profile data and subsequent quality control editing. This allows the profiles to be inspected visually and compared to climatology and neighboring stations. Each data point is associated with data quality codes explained in the GTSPP manuals. Many of the XBT tracks are repeated monthly or annually and allows for investigation of monthly, seasonal, or annual changes in the heat distribution of the upper ocean.

Tropical Atmosphere Ocean/Triangle Trans Ocean Buoy Network (TAO/TRITON) mooring array was originally developed to help predict and measure El Nino events in the Pacific Ocean Basin, but the large dataset has been used for many other studies. Temperature profile data from 36 TAO/TRITON moorings from the equator to 8^{o}S and 140^{o}E to 95^{o}W were extracted for comparison from 1998 to 2014. Because the moorings remain stationary, temporal changes in the dynamics of heat in the ocean can be studied.

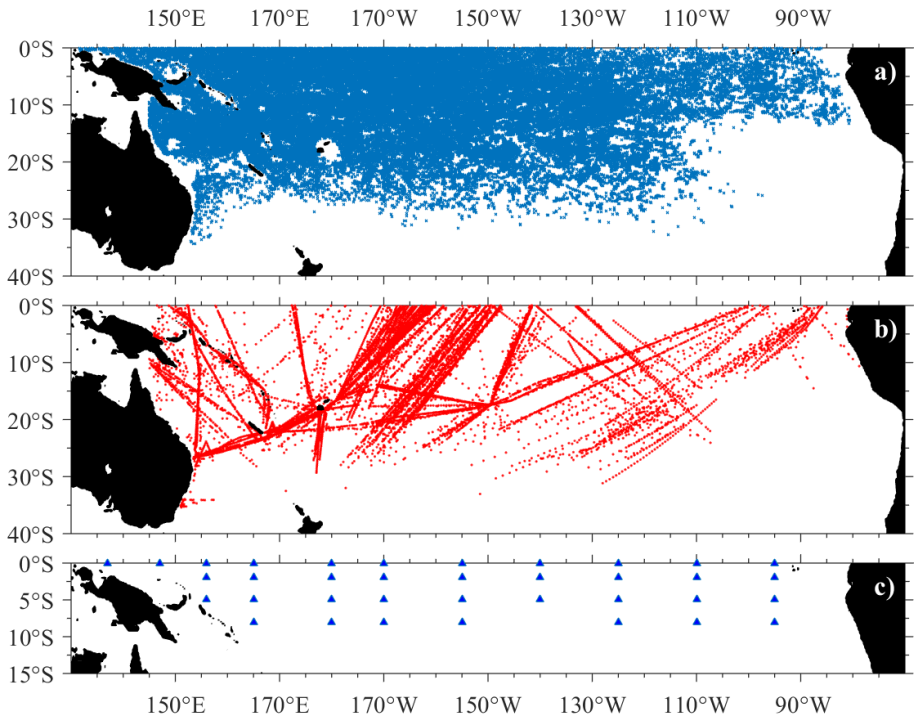

Figure 2-12. Distribution of a) Argo floats, b) XBT transects from research ships and Ships of Opportunity, c) TAO/TRITON moorings used in the evaluation of the OHC algorithm for SPOC.

Quality controlled data from the three platforms were subject to additional quality control once obtained from the monitoring agencies. Similar to the other basins, South Pacific profiles were interpolated to 1-m resolution using a piecewise cubic Hermite interpolating polynomial from 1-m depth to 500-m. The depths of the 20º and 26º isotherms were calculated using a linear interpolation scheme between the 1-m depths around the isotherm. The MLD was defined as the depth at which the temperature exceeds 0.5ºC cooler than the 1-m shallowest depth (Monterey and Levitus, 1997). Finally, OHC was calculated following the method of Leipper and Volgenau (1972).

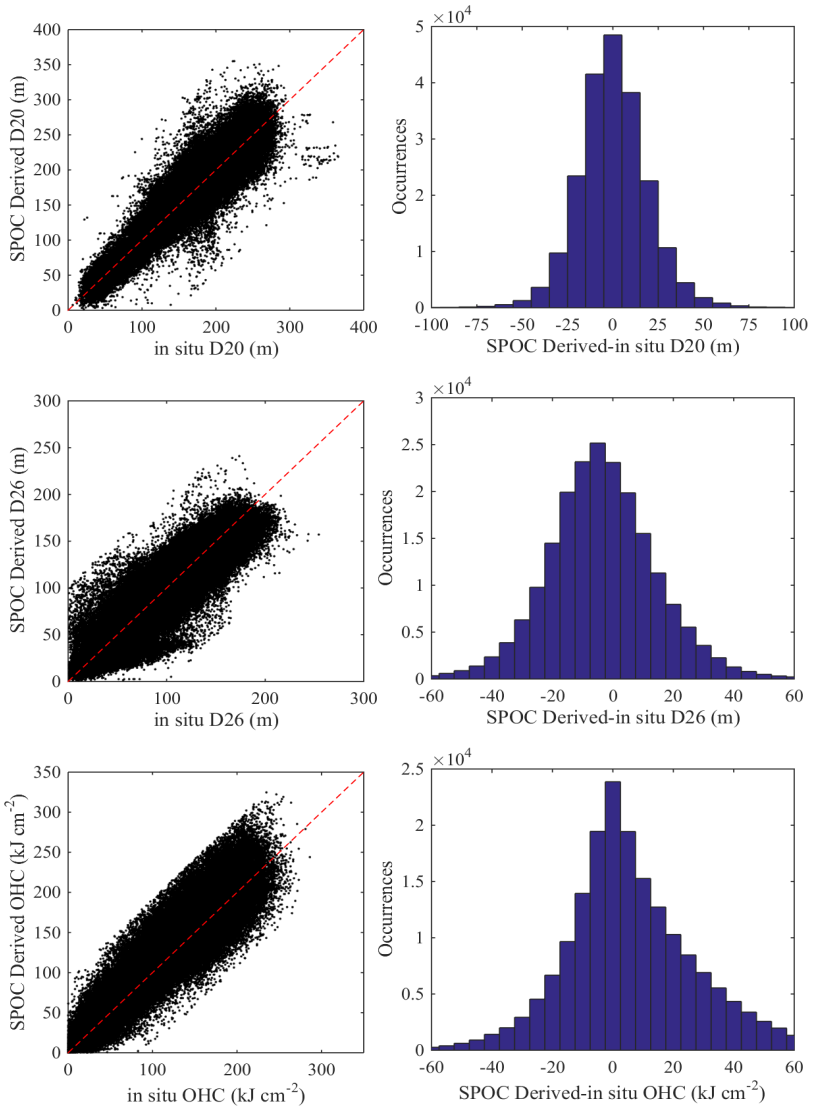

Figure 2-13. Same as Figure 2-8 except for South Pacific Ocean basin using SPOC.

SPOC derived values of D20 show strong correlations to *in-situ* values with normally distributed absolute differences (Figure 2-13 top). Similarly, D26 correlations between SPOC derived and *in-situ* values were close to unity, and their differences evenly distributed (Figure 2-13 middle). OHC comparisons were correlated, with the distributions of the differences normally distributed but with a slight bias where SPOC derived OHC tended to be slightly higher than *in-situ* (Figure 2-13 bottom). RMS differences of D20, D26, and OHC were 18.7 m, 18.5 m, and 23.1 kJ·cm^{-2}, respectively.

2.8 El Nino Considerations

In the evaluation of the D26 regression analysis for both the North and South Pacific basins, an anomalous signal of much deeper *in-situ* values than climatology estimated values of D26 is observed in the analysis (Fig. 2-14 in the circled green area). An investigation by year showed that this signal appeared only in 2002, 2004, 2006, and 2009 of the D26 analysis. A further monthly analysis showed that the anomalous signal corresponded to months during which an El Niño event was occurring. An El Niño event occurs when the westward wind stress in the equatorial Pacific relaxes, allowing the deep surface layer of warm water that normally pools on the western side of the Pacific Ocean basin to spread east. This process results in warmer sea surface temperatures and deeper isotherm depths above the thermocline in the central and eastern tropical Pacific. The points in the green circle represent where the *in-situ* D26 value was much deeper than the GDEM derived D26.

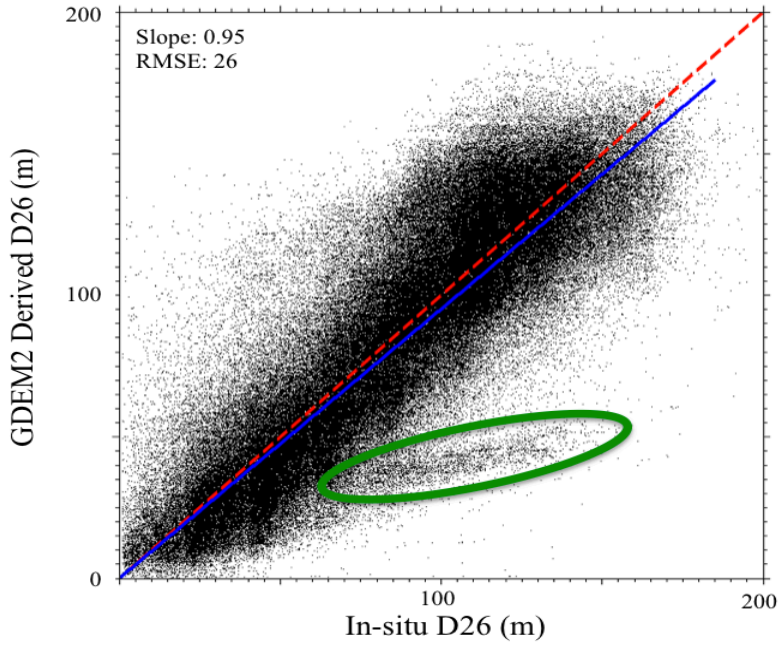

Figure 2-14: Regression analysis of *in-situ* versus GDEM2 climatology derived D26 for the North Pacific Ocean basin from 2000-2011. The red dashed line represents the 1:1 ratio line, the blue line represents the best-fit line, and the green circle highlights the anomalous signal.

The 2002 D26 regression analysis was examined further to verify the El Niño signal. According to National Weather Service Climate Prediction Center, the 2002 El Niño event was strongest through the months of July to December. More detail is shown in Fig. 2-15 where the D26 regression analysis from January to June is on the left and July to December is on the right. The anomalous signal appears only in the months associated with the El Niño event. A regional regression analysis confirmed that the anomalous signal was present in the tropical Pacific region where El Niño ocean anomalies are expected. The anomalous signal occurs below 5^{o}N, in the tropical region, while the signal is absent

above 5ºN. Similar results were seen in the OHC regression analysis but were not shown here. *In-situ* data in comparison with model derived D26 values identified a clear El Niño signal in the tropical North Pacific Ocean basin consistent with the previous studies. Thus the signals are part of the natural oceanic variability rather than erroneous measurements that are accounted for the analysis.

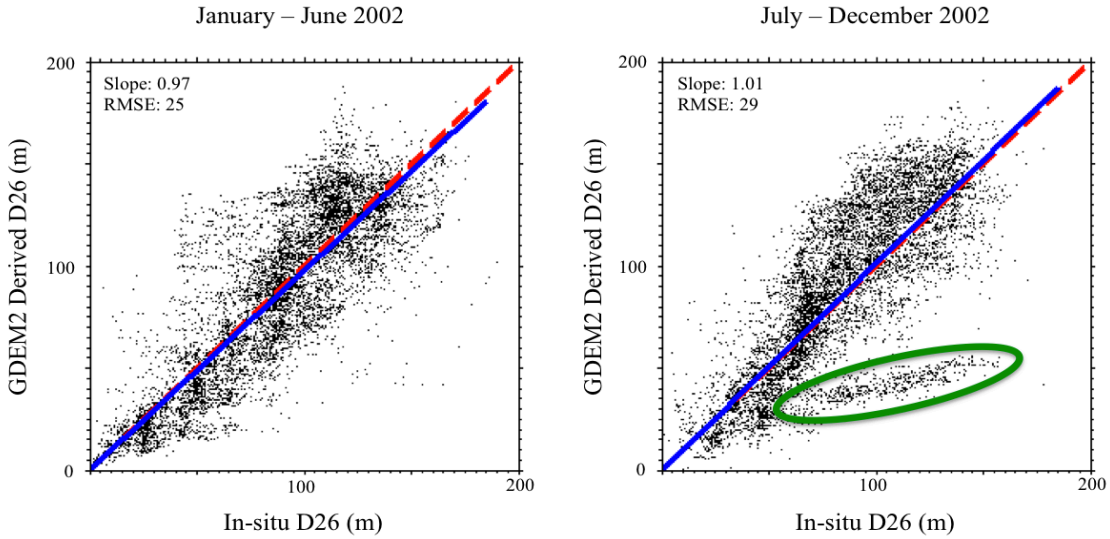

Figure 2-15: Regression analysis of *in-situ* versus GDEM2 climatology derived D26 for the North Pacific Ocean basin for 2002 with January through June on the left and July through December on the right. The red dashed line represents the 1:1 ratio line, the blue line represents the best-fit line, and the green circle highlights the anomalous signal.

2.9 Normalized RMSD in Each Basin

2.9.1 North Atlantic Ocean

To more accurately identify the regions of uncertainty of the 2.5-layer model, a normalized value of RMSD (hereafter NRMSD) was examined. NRMSD (Figure 2-16) is the RMSD as calculated above normalized by the mean of the local *in-situ* observations. Maximum values of NRMSD were typically highest in the GOM and the northern Atlantic Ocean for most variables of interest. D20 had a large NRMSD in the North Atlantic Ocean basin because D20 often ventilates in this region. Even if satellite SSTs were just above 20°C, the calculation of D20 would not be adjusted, leading to large errors and a manifestation of the drawbacks of the simple two-layer model. Additionally, this was an area of high variability due to the GS eddy field, as suggested by the standard deviations of observations (not shown).

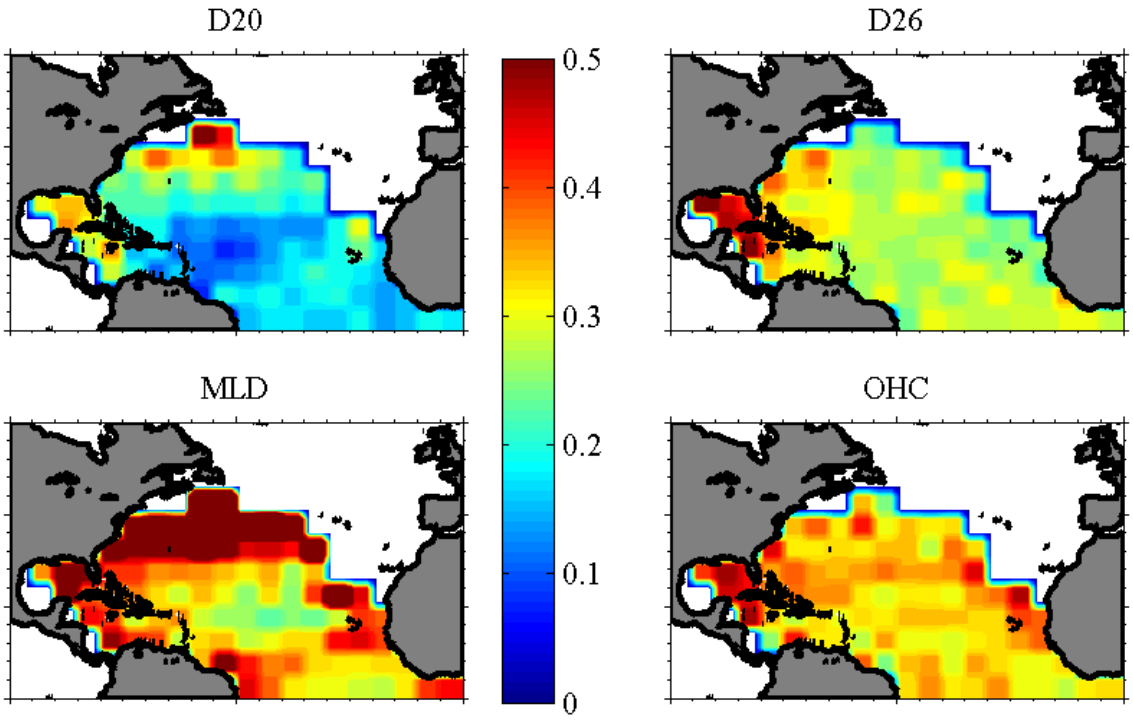

Figure 2-16: Normalized RMSD for D20, D26, MLD, and OHC during the hurricane season. The contours represent the differences relative to the variables' average magnitudes. NRMSD is greatest in the GOM and northern Atlantic.

Mainelli (2000) overestimated D20 throughout the entire basin by over 30 m (Table 2-2). This total bias was essentially negligible (<1 m) with the SMARTS climatology where RMSD was reduced by 37%. In the GOM and LC, Mainelli's bias reduced to about 20 m and the SMARTS bias was still nearly negligible. RMSD was larger in the GOM and LC due to larger depth variability of observations. Implementing SMARTS reduced the RMSD of D20 to about 40 m in the GOM and LC or a reduction of nearly 20%.

Across the entire basin, RMSD values decreased using SMARTS to estimate D26 by 25%, however it should be noted that biases were also of the same magnitude. RMSD decreased from 24 m to 18 m using SMARTS, but where Mainelli (2000) overestimated D26 by about 8 m, SMARTS underestimated D26 by the same magnitude. Similarly in the GOM and LC where significant spatial variability occurs, RMSD was reduced by 25% to about 24 m using SMARTS. In this complex regime, Mainelli overestimated D26 by 11 m in the GOM and LC, while SMARTS underestimated D26 by 11 m.

There were large MLD biases in the Mainelli climatology, underestimating MLD basin-wide by 21 m and overestimating in the LC and GOM by nearly 14 m. Such large differences led to a basin-wide RMSD of 32 m and 23 m in the GOM and LC, respectively. Mainelli's estimation of upper ocean

thermal structure did not utilize a MLD in the algorithm, whereas the updated two-layer model with the SMARTS Climatology uses an adjusted MLD. Using SMARTS reduced basin-wide RMSD by almost 50% and a small negative bias of 4 m. In the GOM and LC, SMARTS improvements were more modest with a negative bias of 6 m and a 20% improvement in RMSD.

Using all *in-situ* data from the entire Atlantic Ocean basin, the Mainelli climatology performed well when calculating OHC, with a bias of less than 1 $kJ \cdot cm^{-2}$ and RMSD of 18 $kJ \cdot cm^{-2}$. SMARTS decreases RMSD to 15 $kJ \cdot cm^{-2}$ with a small 3 $kJ \cdot cm^{-2}$ underestimate. In the region of greatest concern where hurricanes tend to reach severe status in the GOM, Mainelli overestimated OHC by an average of 20 $kJ \cdot cm^{-2}$ in the LC complex whereas the bias from SMARTS was nearly negligible. SMARTS decreased RMSD in the GOM and LC by 35%, from about 40 to 25 $kJ \cdot cm^{-2}$. Such large changes in OHC calculations could have significant impacts on hurricane intensity forecasting in the SHIPS model (DeMaria *et al*., 2005).

Basin RMSD (bias)	D20 (m)	D26 (m)	MLD (m)	OHC (kJ/cm²)
Mainelli	48.9 (34.2)	24.1 (7.7)	32.2 (-21.4)	18.3 (-0.6)
SMARTS Relative	31.0 (-0.5)	18.2 (-8.4)	17.2 (-3.6)	15.0 (-3.0)
SMARTS Absolute	30.2 (-0.7)	17.9 (-7.3)	16.9 (-3.5)	14.8 (-2.6)
GOM RMSD (bias)	D20 (m)	D26 (m)	MLD (m)	OHC (kJ/cm²)
Mainelli	47.6 (17.9)	32.5 (11.4)	22.1 (13.3)	40.1 (21.7)
SMARTS Relative	41.9 (0.6)	24.5 (-11.6)	17.7 (-5.7)	26.1 (-0.5)
SMARTS Absolute	40.7 (-0.8)	24.5 (-12.0)	17.5 (-6.2)	25.5 (-1.1)
LC RMSD (bias)	D20 (m)	D26 (m)	MLD (m)	OHC (kJ/cm²)
Mainelli	49.3 (20.5)	30.9 (11.1)	25.4 (14.0)	36.9 (17.3)
SMARTS Relative	41.3 (-0.3)	23.1 (-10.4)	19.8 (-5.0)	24.7 (-1.4)
SMARTS Absolute	39.8 (-1.5)	22.7 (-10.2)	19.5 (-5.3)	24.0 (-1.6)

Table 2-2: RMSD and bias (in parenthesis) of satellite calculation of upper ocean thermal structure using Mainelli (2000) and the relative and absolute weighted versions of the SMARTS Climatology. Values were calculated using all available *in-situ* observations basin-wide (top), and in the GOM (middle) and LC (bottom).

Given these results of comparing to *in-situ* measurements and to the Mainelli (2000) approach, SMARTS represents realistic estimates of isotherm depths, MLD and OHC. These operational products will be evaluated using temperature profiles over the next several years to update and improve the model and resultant products.

2.9.2 North Pacific Ocean

To more accurately identify the regions of uncertainty of the two-layer model, a normalized value of RMSD (hereafter NRMSD) was examined. NRMSD (Figure 2-17) is the RMSD as calculated above normalized by the mean of the local *in-situ* observations. Maximum values of NRMSD were typically

highest in the GOM and the northern Pacific Ocean for most variables of interest. D20 had a large NRMSD in the North Pacific Ocean basin because D20 associated with the Kuroshio and its extension. If satellite SSTs were just above 20°C, the calculation of D20 would not be adjusted, leading to large errors and a manifestation of the drawbacks of the simple 2.5-layer model. In general the D26 and MLD signals follow a similar pattern except that the NRMSD are also largest in the eastern Pacific due in part to the sharpness of the thermocline in that regime. The buoyancy periods at the base of the MLD in this region often exceeds 20 cycles per hour (cph) where the D26 is between 35 to 40 m for most of the year (Raymond *et al*., 2004; Shay and Brewster, 2010). Further complicating the eastern Pacific Ocean is the presence of the cold tongue extending from the equatorial region to about 6 to 7ºN. Note that the pattern of the NRMSD for OHC follows the MLD more than the other variables, although not nearly as high. Given these patterns, the North Pacific Ocean contains considerable spatial variability that is captured by this measure during the TC season. Similar, but slightly weaker patterns occur during the off-season (not shown).

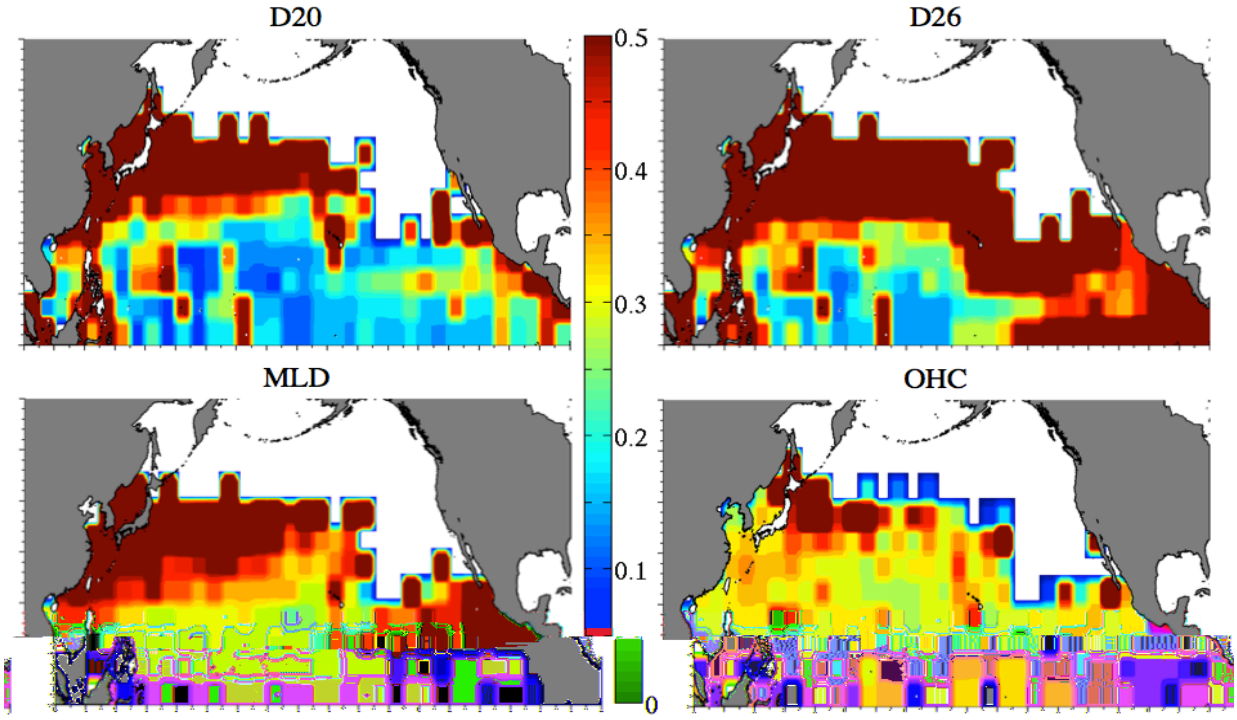

Figure 2-17: Normalized RMSD for D20, D26, MLD, and OHC during the hurricane season. The contours represent the differences relative to the variables' average magnitudes for the North Pacific Ocean Basin.

2.9.3 South Pacific Ocean

The South Pacific Ocean NRMSD (Figure 2-18) is the RMSD as calculated above normalized by the mean of the local *in-situ* observations. During the cyclone season, D20 had large NRMSD in the near island chains, like Fiji, Vanuatu and French Polynesia, and off the coast of Ecuador and Peru. MLD NRMSD was highest in Ecuador/Peru region as well as along the Australian coast and eastward in the eddy rich zone of 30ºS. The NRMSD for D26 and OHC was large for much of the eastern of the domain, due to the sharp thermocline. Areas close to the Australian coast and eastward in the eddy rich zone also had higher D26 and OHC NRMSD.

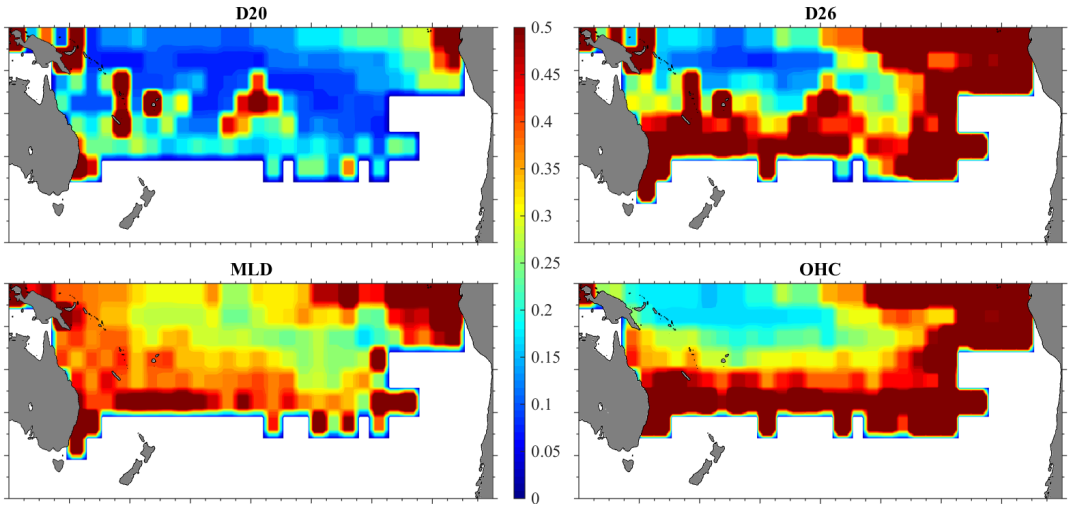

Figure 2-18: Normalized RMSD for D20, D26, MLD, and OHC during the Cyclone season. The contours represent the differences relative to the variables' average magnitudes for the South Pacific Ocean Basin.

2.10 Example Comparisons to Observations in Each Basin

2.10.1 North Atlantic Ocean

To illustrate the temporally evolving characteristics in a Lagrangian framework from the SMARTS approach, isotherm depths, SST and OHC are compared to the fields from Argo profilers. The floats completed one full profile of the water column every 10 days, the same as the time window of SSHA data (e.g., Jason), ensuring a corresponding time series of independently calculated satellite fields (Figure 2-19). The data are from an Argo profiler west of the Caribbean Islands in 2008 with characteristics representative of the full dataset. D20 typically did not change greatly between subsequent profiles, although satellite calculations showed higher temporal variability in D20. The two-layer model's calculation of D20 was sensitive to SSHA changes, overestimating observed *in-situ* changes but still capturing change on a monthly timescale. Satellite-derived values of D26 also showed such overestimated fluctuations, which was expected considering its dependence on D20. *In-situ*

values of D26 fluctuated enough such that climatology alone could not accurately depict the ocean subsurface structures. Generally, the two-layer model accurately determined the change of direction of the 26°C isotherm. Differences in OHC were a result of disparities between *in-situ* and satellite values of D26.

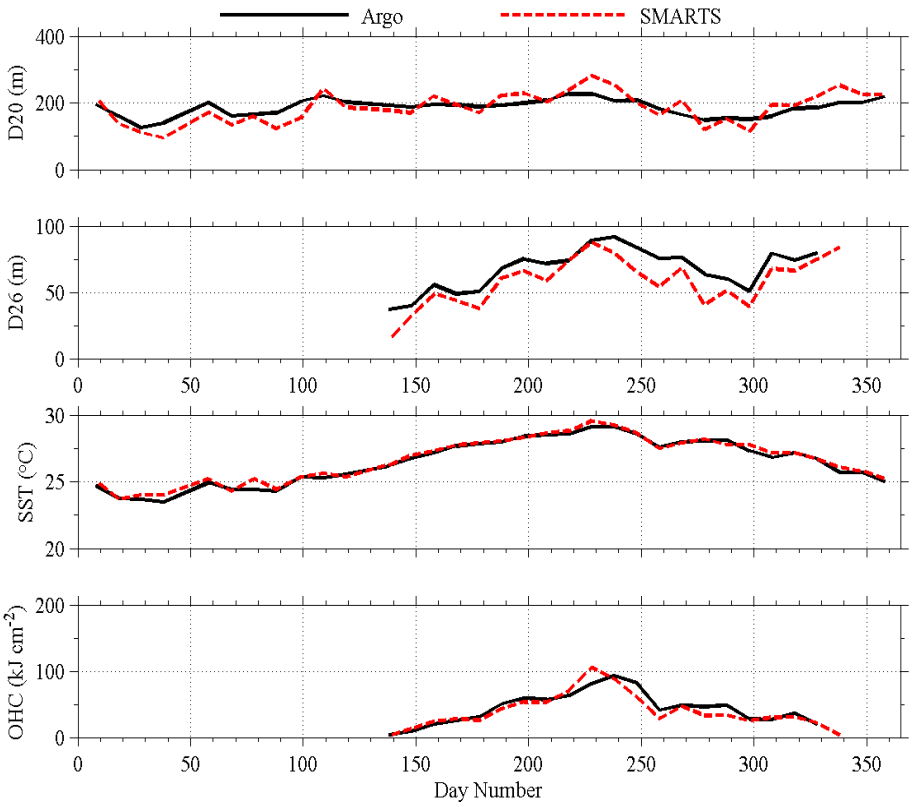

Figure 2-19: Comparisons of D20, D26, SST, and OHC between Argo profiler 4900600 (solid black) and SMARTS-derived (dashed red) from 2008 located north of the Caribbean Islands.

Repeated XBT transects across the Atlantic provided snapshots of vertical temperature structure, which allowed for comparison to SMARTS-derived values. Three annual September transects between 2004 and 2006 across a region east of Florida through the GS provided over 120 XBT profiles for analysis (Figure 2-20). Along this transect, the satellite algorithm using the SMARTS Climatology captured the horizontal variability of OHC within the error of observations. A large fraction of the OHC variability was attributed to east/west SST gradients, considering the D26 was essentially flat. Satellite calculations of D20 had a shallow bias, particularly near local minima along the 20°C isotherm. The satellite methodology accurately calculated the locations of relative maxima and minima of D20, except that the model exaggerated the slope of the D20 surface. However, the locations of maxima and minima were accurate.

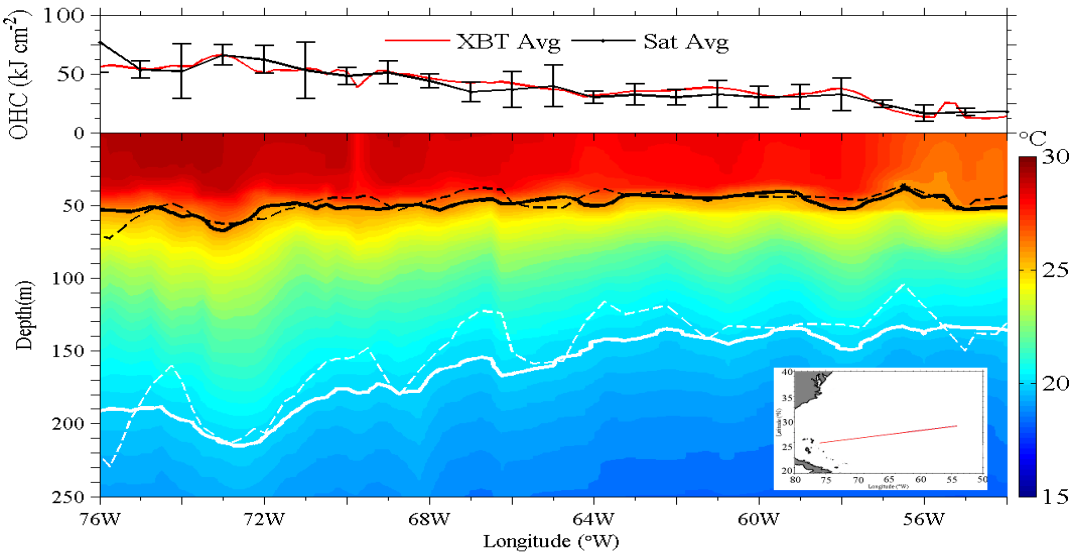

Figure 2-20: Average temperature observed by XBTs along an east-west transect from 25ºN to 28ºN (inset) with observed (solid) and SMARTS-derived (dashed) depths of D26 (black) and D20 (white). Observed OHC (red line, top) is compared to satellite derived values with error bars equivalent to 2σ.

2.10.2 North Pacific Ocean

TAO/TRITON and SPORTS derived D20, D26, MLD, SST, and OHC were averaged over a twelve-year period (2000-2011) to obtain the daily averaged values over the year (Figure 2-21). Seasonally, SPORTS under estimates D26, and therefore OHC, in the winter and spring. In the summer and fall, during the most active part of the tropical cyclone season, SPORTS does a better job of estimating D26 and OHC. Over the most year time period, the TAO/TRITON mooring data falls within one standard deviation from the SPORTS derived variables. This is especially true during the latter half of the year, during the peak of tropical cyclone season. The seasonality of OHC can clearly be seen as well with a peak in the fall and a minimum in the late winter.

The two-layer model uses the SSHA to estimate the D20; then the MLD and D26 are found using the SPORTS climatology. Small fluctuations away from TAO/TRITON mooring D20 seen in the SPORTS derived D20 become exaggerated in the MLD and D26 derived variables. The underestimation of SPORTS MLD and D26 lead to an underestimation in the SPORTS OHC. Despite the underestimation, SPORTS still manages to accurately estimate the trend in changes of OHC over the year with only small departures from the calculated TAO/TRITON OHC.

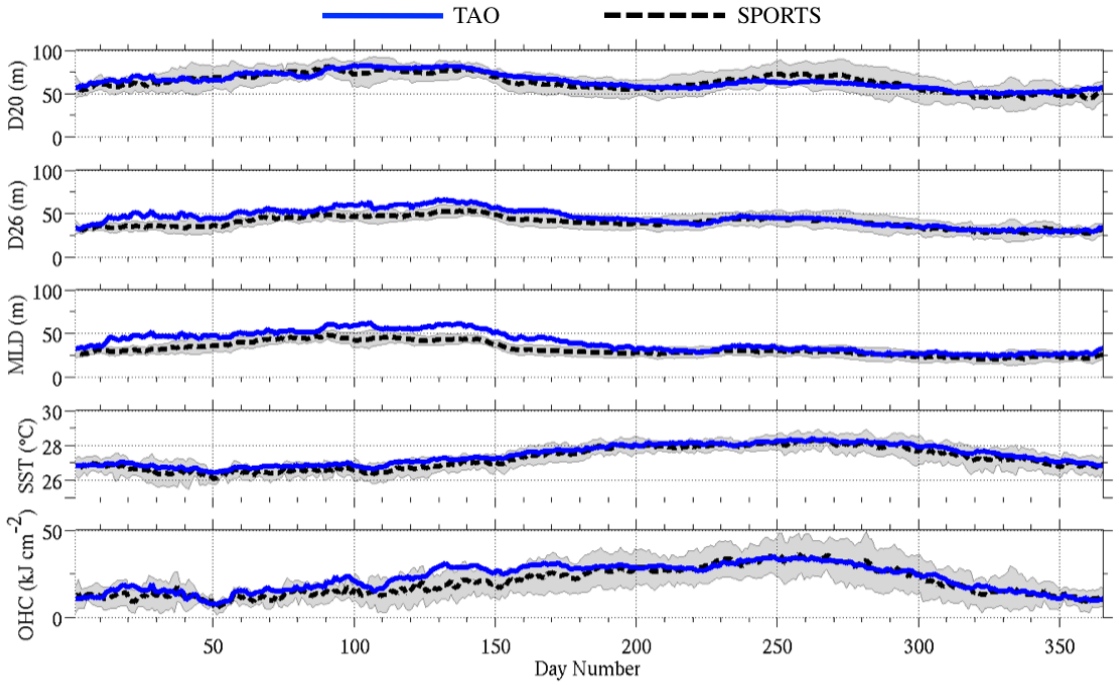

Figure 2-21: A 12-yr averaged time series comparisons of D20, D26, MLD, SST, and OHC from TAO/TRITON mooring at 9°N, 140°W in the central Pacific Ocean where the uncertainty (gray shaded) is represented by error bars equivalent to 1σ over the 12-year period of concurrent *in-situ* and satellite measurements.

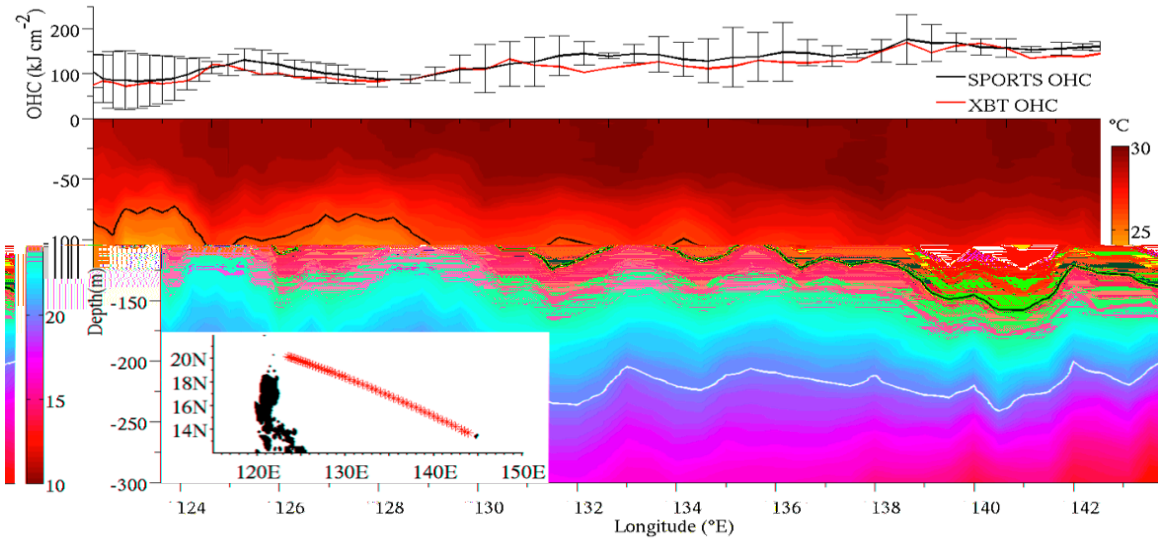

Figure 2-22: Same as Figure 2-20 except for the North Pacific XBT transect from SPORTS from 14 to 20°N (see inset) in the western Pacific Ocean.

The average OHC from repeat XBT transect along a ship track from Guam to the Philippines in the Philippine Sea (Figure 2-21 inset) and the corresponding average SPORTS OHC were averaged over the month of September for a three-year period from 2008-2010 (Figure 2-21). As evident from the transect spacing, data were sampled at a higher resolution in the western portion of the transect. Possible reasoning for this could correspond to stronger eddies existing in the western Philippine Sea. The shear instability generated by the opposing flows of the Subtropical Countercurrent and North Equatorial Current help provide energy for the eddies to intensify as they propagate westward in this region. The cold and warm eddies can be seen at 125°E and 139°E. The stronger, fluctuating eddies in the western Philippine Sea cause more variance in this area.

2.10.3 South Pacific Ocean

To investigate the Eulerian view of heat distribution in the upper ocean, TAO/TRITON and SPOC derived D20, D26, MLD, SST, and OHC were averaged over a 17-year period (1998-2014) to obtain daily averaged values over the year (Figure 2-23). During the cyclone (off) season, SPOC overestimated (underestimated) D20, but remained within the 1σ error. D26 was overestimated during the cyclone season, but follows the mooring D26 closely. Satellite SST followed very closely

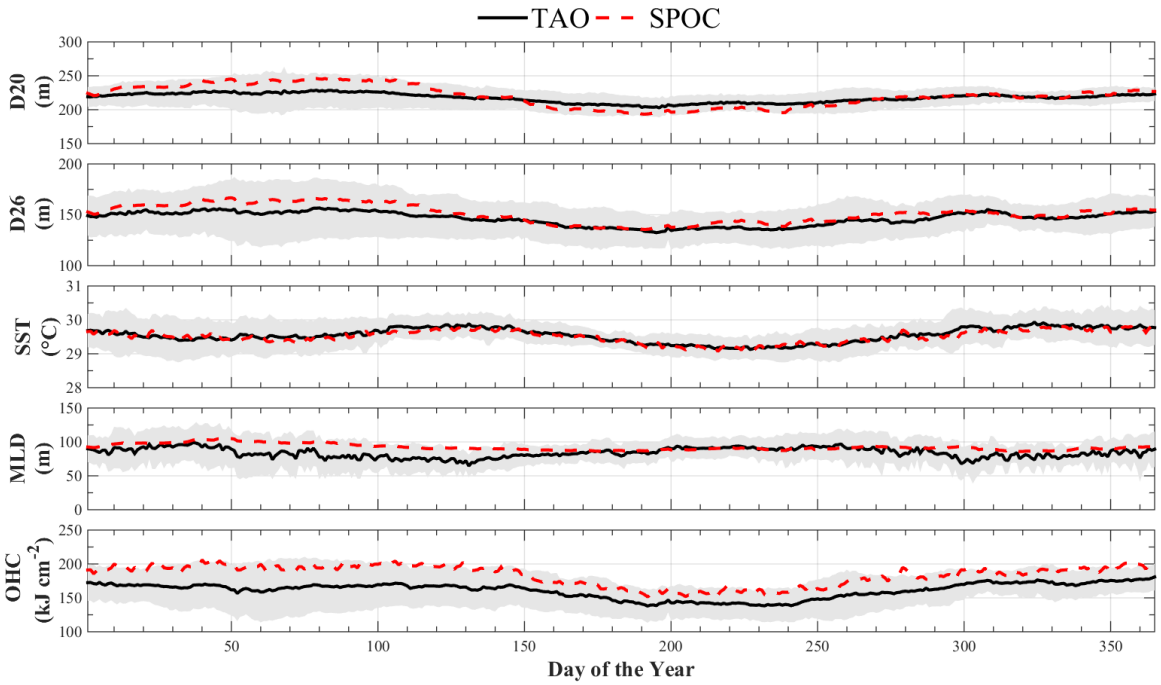

Figure 2-23: A 17-year averaged time series comparisons of D20, D26, MLD, SST, and OHC from the TAO/TRITON mooring at 8°S, 180° in the central Pacific Ocean. Uncertainty (gray shaded) represents error bars equivalent to 1σ over the 17-year period of concurrent *in-situ* and satellite measurements.

to the mooring SST and well within the error. MLD was slightly overestimated near the end of the cyclone season/beginning of the off season, but followed relatively closely to the mooring's average MLD. SPOC consistently overestimated the OHC throughout the year. For all of the cyclone season, the variability was higher during the cyclone season as evidenced in the error.

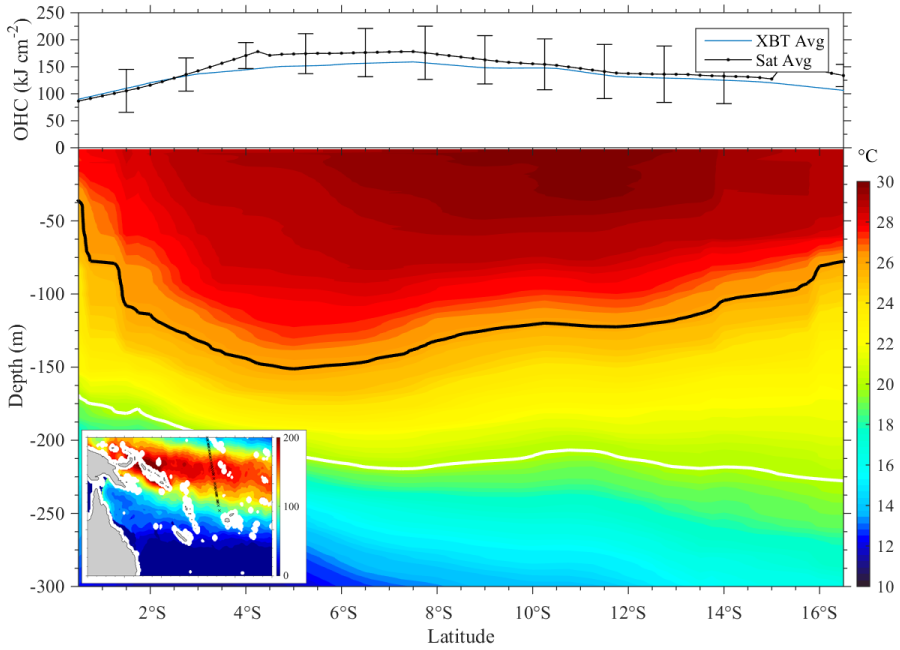

Figure 2-24. Same as Figure 2-22 except a north-south XBT transect and SPOC-derived depths from 18ºN to 0º (inset) in the western South Pacific Ocean.

Thermal structure from locations along an XBT transect (Figure 2-24 inset) during April from Fiji to the Equator were averaged for four years, 1998-2002 (Figure 2-24 bottom). The heat structure shows a deep pool skewed towards the equator (5ºS) with the highest temperatures around 30ºC at 11.5ºS. D26 tends to follow the bottom of the warm pool, with deeper (shallower) depths in the north (south), while D20 tends to deepen away from the equator when D26 starts to shallow. Average satellite derived OHC from 1998-2002 during the month of April and average OHC from 5 annual XBT transects reflect the warm pool at 5ºN and while SPOC tends to overestimate the OHC, it remains well within the error estimates.

3. ASSUMPTIONS AND LIMITATIONS

3.1 Performance Assumptions

The original premise of this OHC product derived from climatologies and satellite data was to at least provide forecasters with an idea where the sources and sinks of OHC were located relative to the

projected track of hurricanes. Subsequently, the original approach of Mainelli (2000) was brought into SHIPS to assess whether it made a difference to the forecast. As per Mainelli et al. (2008), OHC made a large impact on Hurricane Ivan (2004). At that point, the approach became much more quantitative since the threshold in SHIPS was set to 60 kJ·cm-2 for OHC to become important.

The basic underlying assumption is that the ocean has an active upper layer with more of an inert lower layer where the key isotherm depth is the 20°C (e.g., Goni *et al.*, 1996). Based on measurements over the basin, this is approximately correct. However, in the GOM's Loop Current, convergence begins at 20°C. In the Gulf Common Water and STW, one could also argue that it's the 18°C based on AXCTD profiles (Figure 3-1). In the layer above this level, we assume that the layer is density compensating by the salinity field (which is really not included in the algorithm per se due primarily to the lack of salinity profiles). Thus, changes to the thermal structure will be compensated by changes in the salinity to maintain a relatively constant density of the upper layer from which we estimate reduced gravity between the two layers.

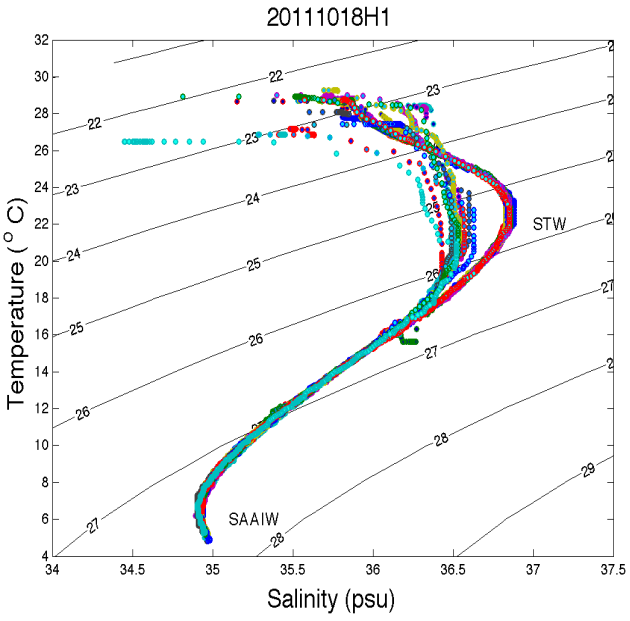

Figure 3-1: Temperature and salinity diagrams for AXCTDs deployed during a LC survey over the GOM in October 2011 from NOAA WP-3D. Solid contours are sigma-t. The water masses are marked accordingly where the STW (subtropical water) emanates from the Caribbean Sea and is the classic signature of the LC and WCR and SAAIW is Sub Antarctic Intermediate Water.

In addition, the ocean mixed layer sits on top of this upper layer which has a relationship to the 20°C isotherm. The *in-situ* data suggests similar behavior, and changes in the thermocline thicknesses can make small adjustments (~3 to 5%) to the MLD. That said, what is lacking is the relationship to surface forcing such as heat fluxes and the wind stress which affects SST as well as the MLD changes. In addition, current shear at the base of the layer which is the biggest contributor to ocean mixed layer

cooling is also not included (Jacob et al., 2000). This must be relegated to the full three dimensional ocean models such as HYCOM, not this product (Halliwell et al. 2008; 2011).

Idealized temperature profiles can have significant deviations as we observed during the Deep Water Horizon measurements (Shay et al., 2011). That is, the approach does not account for seasonal subsurface thermostads. For example, in late winter when MLD is greatest, surface waters are gradually heated due to sensible heating at the surface. This warmer surface water does not mix with the subsurface cooler waters from the winter mixed layer until a strong wind forcing event or internal forcing occurs. WOA and GDEM climatologies (or SMARTS) do not resolve these subsurface thermostads in the monthly climatology (Meyers, 2011).

3.2 Potential Improvements

Hurricanes are a problem that is not going to go away. Moreover, it is getting clearer with even statistical-dynamical models such as SHIPS, that the upper ocean plays a role on hurricane intensity change. Moreover, there a few areas in the North Atlantic Ocean basin, mainly the northwest Caribbean sea, eastern GOM and north of the Caribbean Islands where rapid intensification occurs (Kaplan *et al*., 2009). Because the ocean does not significantly cool in these regimes, more heat is available to hurricanes that often reach severe status (Shay *et al*., 2000).

Over the course of the development and testing, it became clear the biggest limitation to the work are the climatologies that often depart significantly from *in-situ* profiles given the level of smoothing that is performed. These climatologies such as GDEM and WOA are useful at providing profiles in data sparse areas. However, regions of significant variability exist, particularly along fronts and eddies.

A large potential improvement could be made if more data profiles become available through profiling floats, drifters (with thermistor chains), gliders, XBT transects, AXBTs (AXCTDs) and even animal-borne sensing CTD tags. In that scenario, direct relationships could be made to the SSHA field without the need to use a two-layer model. Even with a data base of ~50,000 profiles in the North Atlantic Ocean basin, a simple Baysian Approach relating SSHA to *in-situ* data had 30% more error than SMARTS. Thus, more T/S profiles are needed to relate subsurface density structure to the SSHA and SSH fields. This will take a sizeable investment in oceanographic observing to acquire the profiles needed to resolve ocean structure. If this were to become a reality, the 2.5-layer approach could be replaced with continuously stratified approach, which would decrease the retrieval errors. Notwithstanding, this may be prohibitively expensive over the global ocean. In the absence of this investment, we have to relax back to climatologies.

4. REFERENCES

Bailey, R., A. Gronell, H. Phillips, G. Meyers, and E. Tanner, 1994: CSIRO cookbook for quality control of expendable bathythermograph (XBT) data. *CSIRO Marine Laboratories Report,* No. 220, 75 pp.

Bane, J. M., Jr., and M. H. Sessions, 1984: A field performance test of the Sippican Deep Aircraft-Deployed Expendable Bathythermograph, *J. Geophys. Res.*, **89(C3)**, 3615–3621.

Carval, T., B. Keeley, Y. Takatsuki, T. Yoshida, S. Loch, C. Schmid, R. Goldsmith, A. Wong, R. McCreadie, A. Thresher, and A. Tran, 2010: Argo data management user's manual. Argo Data Management Team, 83 pp.

Chelton, D., and M. G. Schlax, 1996: Global observations of oceanic Rossby waves, *Science,* **272,** 234-238.

Cheney, R., L. Miller, R. Agreen, N. Doyle, and J. Lillibridge, 1994:, TOPEX/Poseidon: The 2-cm solution. *J. Geophys. Res*., **99,** 24,555-24,563.

Cronin, M. F., N. Bond, C. Fairall, J. Hare, M. J. McPhaden, and R. Weller, 2002: Enhanced oceanic and atmospheric monitoring underway in the Eastern Pacfic. *EOS,* **83(19**), 210-211.

de Boyer Montégut, C., G. Madec, A. S. Fischer, A. Lazar, and D. Iudicone, 2004: Mixed layer depth over the global ocean: An examination of profile data and a profile-based climatology, *J. Geophys. Res.*, **109**, C12003.

DeMaria, M. Mainelli M., L.K. Shay, J.A. Knaff, and J. Kaplan, 2005: Further improvements to the statistical hurricane intensity prediction scheme (SHIPS). *Wea. and Forecasting,* **20(4)**, 531-543.

Fox, D. N., W. J. Teague and C. N. Barron, 2002: The Modular Ocean Data Assimilation System (MODAS). *J. Atmos. and Oceanogr. Tech.*, **19**, 240-252.

Freitag, H.P., T.A. Sawatzky, K.B. Ronnholm, and M.J. McPhaden, 2005: Calibration procedures and instrumental accuracy estimates of next generation ATLAS water temperature and pressure measurements. NOAA Tech. Memo. OAR PMEL-128, NTIS: PB2008-101764, NOAA/Pacific Marine Environmental Laboratory, Seattle, WA, 22 pp.

Johnson, G. C., 1995: Revised XCTD fall rate equation coefficients from CTD data. *J. Atmos. and Oceangr. Tech.*, **12**, 1367-1373.

Goni, G. J., S. Kamholz, S. L. Garzoli, and D. B. Olson, 1996: Dynamics of the Brazil/Malvinas confluence based on inverted echo sounders and altimetry. *J. Geophys. Res.*, **95,** 22103-22120.

Halliwell, G., L. K. Shay, S. D. Jacob, O. Smedstad, and E. Uhlhorn, 2008: Improving ocean model initialization for coupled tropical cyclone forecast models using GODAE nowcasts. *Mon Wea Rev,* **136 (7)**, 2576–2591.

Halliwell, G. R., L. K. Shay, J. Brewster, and W. J. Teague. 2011: Evaluation and sensitivity analysis to an ocean model response to hurricane Ivan. *Mon. Wea. Rev*., **139(3),** 921-945.

Harris, A. and E. Maturi, 2012: Geo-Polar Blended Sea Surface Temperatures: Algorithm Theoretical Basis Document, V2.0, NOAA National environmental Satellite Data Information System, Center for Satellite Applications and Research, Camp Springs, VA, 43pp.

Jacob, S.D., L.K. Shay, A.J. Mariano and P.G. Black, 2000: The 3-D oceanic mixed-layer response to Hurricane Gilbert. *J. Phys. Oceanogr.*, **30(6)**, 1407-1429.

Jacob, S. D., and L. K. Shay, 2003: The role of oceanic mesoscale features on the tropical cyclone–induced mixed layer response. *J. Phys. Oceanogr.,* **33,** 649–676.

Jaimes, B., and L. K. Shay, 2009: Mixed layer cooling in mesoscale oceanic eddies during hurricanes Katrina and Rita. *Mon. Wea. Rev.*, **137**, 4188-4207.

Jaimes, B and L. K. Shay, 2010: Near-Inertial Wave Wake of Hurricanes Katrina and Rita over Mesoscale Oceanic Eddies. *J. Phys. Oceanogr.*, **40**, 1320–1337.

Kaplan, J. M. DeMaria, and J. A. Knaff, 2010: A Revised Tropical Cyclone Rapid Intensification Index for the Atlantic and Eastern North Pacific Basins. *Wea. Forecasting*, **25**, 220–241.

Leipper, D. F., and D. Volgenau, 1972: Hurricane heat potential of the Gulf of Mexico. *J. Phys. Oceanogr*., **2**, 218–224.

Lillibridge, J., R. Scharroo, G. Jacobs, L. Russell, and V. Tabor, 2011. Quality Assessment of the Jason-2 Operational and Interim Geophysical Data Records. *Marine Geodesy*, **34**, 191–213.

Mainelli, M., 2000: On the role of the upper ocean in tropical cyclone intensity change. M.S. Thesis, Division of Meteorology and Physical Oceanography, RSMAS, University of Miami, Miami, FL, 73 pp.

Mainelli, M., M. DeMaria, L.K. Shay, and G. Goni, 2008: Application of oceanic heat content estimation to operational forecasting of recent Atlantic Category 5 hurricanes. *Wea. Forecasting*, **23**, 3-16.

Mariano, A. J. and O. B. Brown, 1992: Efficient objective analysis of dynamically heterogeneous and nonstationary fields via the parameter matrix. *Deep-Sea Res.*, **39**, 1255–1271.

McCaskill, E. C., L. K. Shay, J. K. Brewster, and P. Meyers. Creation of the systematically merged Pacific Ocean temperature and salinity (SPORTS) climatology for typhoon intensity forecasts. *J. Atmos. Oceanogr. Tech* , **33(10),** 2259-2272.

Meyers, P. C., 2011: Development and Analysis of the Systematically Merged Atlantic Region Temperature and Salinity Climatology for Satellite-Derived Ocean Thermal Structure. *M.S. Thesis*,

Division of Meteorology and Physical Oceanography, RSMAS, University of Miami, Miami, FL, 33149, 99 pp.

Meyers, P. C., L. K. Shay, and J. K. Brewster, 2014: Development and Analysis of the Systematically Merged Atlantic Regional Temperature and Salinity Climatology for Oceanic Heat Content Estimates. *J. Atmos. Oceanic Technol.*, **31**, 131–149.

Meyers, P. C., L. K. Shay, J. K. Brewster, and B. Jaimes, 2015: Thermal ocean structure response during Hurricanes Gustav and Ike, J. Geophys. Res., **120,** DOI 10.100212015JC010912, 1-18 pp.

Millero, F. J. and Poisson, A. 1981: International one-atmosphere equation of state of seawater. *Deep-Sea Research*, 28A, 625-629.

Monterey, G. I., and S. Levitus, 1997: Climatological cycle of mixed layer depth in the world ocean. U.S. Gov. Printing Office, *NOAA NESDIS*, 5pp.
Palmen, E., 1948: On the formation and structure of tropical cyclones. *Geophysika,* 3, 26–38.

Pun, I-F, I-I Lin, C. -R. Wu, D. -S. Ko, W. -T. Liu, 2007: Validation and Application of Altimetry derived Upper Ocean Thermal Structure in the Western North Pacific Ocean for Typhoon Intensity Forecast. *IEEE Trans. Geosci. Rem. Sens*., **45**, 1616-1630.

Raymond, D. J., S. K. Esbensen, C. Paulson, M. Gregg, C. Bretherton, W. A. Peterson, R. Cifelli, L. Shay, C. Ohlmann, and P. Zuidema, 2004: EPIC2001 and the coupled ocean-atmosphere system of the tropical East Pacific. *Bull. Amer. Met. Soc.*, **85(9),** 1341-1354.

Rudzin, J., L. K. Shay, B. Jaimes, and J. K. Brewster, 2017: Upper ocean observations in the eastern Caribbean Sea reveal barrier layer within a warm core eddy. *J. Geophys. Res. Oceans*, **122,** doi:10.1002/2016JC012339, 1057-1071.

Scharroo, R, W.H. Smith, and J.L. Lillibridge 2005: Satellite Altimetry and the Intensification of Hurricane Katrina. *EOS,* **86**, 366-367.

Servain, J., A. J. Busalacchi, M. J. McPhaden, A. D. Moura, G. Reverdin, M. Vianna, and S. E. Zebiak, 1998: A Pilot Research Moored Array in the Tropical Atlantic (PIRATA). *Bull. Amer. Meteor. Soc.*, **79**, 2019–2031.

Shay, L.K., G.J. Goni and P.G. Black, 2000: Effects of a warm oceanic feature on Hurricane Opal. *Mon. Wea. Rev.*, **125(5)**, 1366-1383.

Shay, L. K., and E. Uhlhorn, 2008: Loop Current response to hurricanes Isidore and Lili, *Mon. Wea Rev.*, **137**, 3248-3274

Shay, L. K., and J. K. Brewster, 2010: Eastern Pacific oceanic heat content estimation for hurricane intensity forecasting. *Mon. Wea. Rev.,* **138**, 2110-2131.

Shay, L. K., B. Jaimes, J. K. Brewster, P. Meyers, C. McCaskill, E. W. Uhlhorn, F. D. Marks, G. R. Halliwell, O. M. Smedsted and P. Hogan, 2011: Airborne surveys of the Loop Current complex from NOAA WP-3D during the Deep Water Horizon oil spill. AGU Geophysical Monograph Series, *Monitoring and Modeling the Deep Water Horizon Oil Spill: A Record Breaking Enterprise*, eds Y. Liu, D. Streets and R. W. Weisberg, **195**, 131-151.

Singer, J.J., 1990: On the error observed in electronically digitized T-7 XBT data, *J. Atmos. Oceaogr. Tech.*, **7**, 603-611.

Teague, W.J., M.J. Carron, and P.J. Hogan, 1990: A comparison between the Generalized Digital Environmental Model and Levitus climatologies. *J. Geophys. Res*., **95,** 7167-7183.

END OF DOCUMENT